UNIVERSITI TEKNOLOGI MARA

MATHEMATICAL MODELLING OF POWELL-EYRING HYBRID NANOFLUID FLOW WITH VARIOUS FACTORS

NUR ARIF HUSAINI BIN NORWAZA

MSc

November 2025

UNIVERSITI TEKNOLOGI MARA

MATHEMATICAL MODELLING OF POWELL-EYRING HYBRID NANOFLUID FLOW WITH VARIOUS FACTORS

NUR ARIF HUSAINI BIN NORWAZA

Proposal submitted in fulfilment
of the requirements for the degree of
Master of Science (Mathematics)

Faculty of Computer and Mathematical Sciences

November 2025

CONFIRMATION BY PANEL OF EXAMINERS

I certify that a Panel of Examiners has met on 7 November 2025 to conduct the Defence Research Proposal (DRP) of Nur Arif Husaini Bin Norwaza on his Masters of Science thesis entitled "Mathematical Modelling of Powell-Eyring Hybrid Nanofluid Flow with Various Factors". The Panel of Examiner recommends that the student be allowed to proceed with the research. The Panel of Examiners was as follows:

PM DR SHAHARUDDIN CIK SOH, PhD
Associate Professor
Faculty of Computer and Mathematical Sciences
Universiti Teknologi MARA

DR MOHD RIJAL BIN ILIAS, PhD
Senior Lecturer
Faculty of Computer and Mathematical Sciences
Universiti Teknologi MARA

DR NUR ARDIANA BINTI AMIRSOM, PhD
Senior Lecturer
Faculty of Computer and Mathematical Sciences
Universiti Teknologi MARA

DR NOR FADHILAH BINTI DZULKIFLI, PhD
Senior Lecturer
Faculty of Computer and Mathematical Sciences
Universiti Teknologi MARA

PROF DR HJH ZURAEDA IBRAHIM
Dean
Institute of Postgraduates Studies
Universiti Teknologi MARA

Date: 7 November 2025

AUTHOR'S DECLARATION

I declare that the work in this thesis was carried out in accordance with the regulations of Universiti Teknologi MARA. It is original and is the results of my own work, unless otherwise indicated or acknowledged as referenced work. This proposal has not been submitted to any other academic institution or non-academic institution for any degree or qualification.

I, hereby, acknowledge that I have been supplied with the Academic Rules and Regulations for Postgraduate, Universiti Teknologi MARA, regulating the conduct of my study and research.

Name of Student	:	NUR ARIF HUSAINI NORWAZA
Student ID. No.	:	2025763013
Programme	:	Master of Science (Mathematics) - CDCS752
Faculty	:	Faculty of Computer and Mathematical Sciences
Thesis Title	:	Mathematical Modelling of Powell-Eyring Hybrid Nanofluid Flow with Various Factors
Signature of Student	:	……..
Date	:	November 2025

ABSTRACT

Hybrid nanofluids have gained increasing attention for their enhanced heat transfer capabilities compared to traditional mono nanofluids, especially in energy systems like solar collectors. Many studies agree that the size, shape, and material of nanoparticles play a significant role in determining how well these fluids perform thermally. However, when these nanofluids exhibit non-Newtonian behaviour, such as shear-thinning and are exposed to complex influences like magnetic fields, Joule heating and thermal radiation, their behaviour becomes much harder to predict. In particular, the Powell-Eyring model, which is well-suited for describing non-Newtonian fluids from shear-thinning perspective, has not been widely applied to hybrid nanofluid flows. There is still debate within the research community over which modelling approaches and numerical methods produce the most reliable results, especially when analysing Powell-Eyring hybrid nanofluids under conditions involving magnetohydrodynamics (MHD) and thermal radiation. Some studies suggest that applying a magnetic field on an inclined surface can enhance heat transfer through Joule heating and improved temperature distribution, while others emphasize its suppressive effect on fluid motion due to the Lorentz force, which may ultimately reduce the overall rate of heat transfer. Additionally, although numerical methods function provided by MATLAB such as bvp4c are widely employed, concerns persist regarding their accuracy when applied to stiff systems, where numerical solutions may become inefficient unless extremely small step sizes are used, and to highly non-linear systems, in which the dependent variables or their derivatives appear in multiplicative or non-proportional relationships. This research proposes to develop a mathematical model that captures the flow of a Powell-Eyring hybrid nanofluid over multiple flow medium, surface orientation, while considering effects such as magnetic fields, thermal radiation, Joule heating, mixed convection, and suction or injection. The resulting system of equations will be solved using a backward differentiation formula (BDF), and the results will be compared with those obtained from MATLAB's bvp5c solver to verify accuracy. The central hypothesis is that using a non-Newtonian model like Powell-Eyring, will provide a clearer and more accurate understanding of how these nanofluids behave in real-world engineering conditions. It is anticipated that early results will show that certain combinations of nanoparticle types, magnetic field strengths, and surface effects can improve heat transfer significantly, making these models highly useful for future thermal system designs.

ACKNOWLEDGEMENT

Firstly, I wish to thank God for giving me the opportunity to embark on my Master and for completing this proporsal successfully. My gratitude and thanks go to my supervisor Dr. Iskandar Shah Bin Mohd Zawawi, internal co-supervisor Dr. Nur Syazana Binti Anuar.

TABLE OF CONTENTS

LIST OF TABLES

LIST OF FIGURES

CHAPTER 1
INTRODUCTION

1.1 Research Background

Globally, there is an increasing demand for cleaner and more sustainable energy sources. Among the various renewable options, solar energy stands out as one of the most promising, particularly when harnessed through solar thermal systems such as flat-plate and parabolic trough collectors. However, these systems face a persistent limitation: conventional heat transfer fluids such as water, and various oils exhibit relatively low thermal conductivity. Inefficient heat transport within these fluids leads to significant energy losses, reducing overall system performance. Consequently, researchers have been driven to explore advanced working fluids with enhanced thermophysical properties to improve the efficiency of solar thermal systems.

One significant advancement in thermal science has been the development of nanofluids, base liquids engineered with the dispersion of nanoparticles, typically composed of materials such as copper, alumina, or carbon nanotubes. Even at very small concentrations, these particles give the fluid a dramatic boost in thermal conductivity. Taking it a step further, researchers began combining two different nanoparticles to form hybrid nanofluids. This approach harnesses the strengths of each particle type and often outperforms single particle nanofluids. However, it still unclear on what is the best combination of nanoparticles, what concentration works best, and how do we keep these mixtures stable in the long run?

Another important question concerns how these fluids behave under applied stress. Many engineering systems do not adhere to the simple, linear characteristics of Newtonian fluids. Instead, they exhibit behaviour typical of non-Newtonian fluids, in which viscosity varies with the rate of shear. The Powell-Eyring model is particularly well suited to describing such behaviour, as it realistically captures shear-thinning effects while maintaining consistency with Newtonian behaviour under limiting conditions. Interestingly, despite these advantages, the model has not been widely

applied in the study of hybrid nanofluids; most existing research continues to rely on more simplified rheological models.

Furthermore, existing studies are still not good enough when considering more complex real-world conditions. In actual solar collectors, magnetic fields, Joule heating, thermal radiation, and Newtonian wall heating can all interact at the same time. Magnetic fields slow the flow through Lorentz forces but can raise temperatures; Joule heating introduces extra energy through resistance; radiation at high surface temperatures reshapes heat flux; and Newtonian heating at the wall alters how energy transfers between the solid and the fluid. Add in surface inclination or roughness, and we will get a system that is far richer, but also far harder to predict.

Solving the governing equations for these fluid flows presents considerable mathematical challenges. Classical numerical solvers, such as the Runge-Kutta family or MATLAB's bvp4c routine, often encounter difficulties when the equations exhibit strong stiffness or pronounced nonlinearity. Although more stable approaches, such as the backward differentiation formula (BDF), are available, their application to these problems remains relatively unexplored. This methodological gap introduces uncertainty not only in theoretical analyses but also in practical design, as engineers may rely on models that fail to accurately capture the real behaviour of solar thermal systems.

This study aims to create a more realistic and reliable mathematical model: by considering the Powell-Eyring model, hybrid nanofluids, and the combined effects of magnetohydrodynamics, Joule heating, radiation at various surface orientation. At the same time, by testing accurate numerical solvers like BDF against existing methods, the study seeks to introduce a new alternative approach for handling stiff and highly nonlinear boundary-layer problems.

1.2 Heat Transfer

Heat is a process of energy transfer from one system to another (Rennie & Law, 2019). As it is a transient phenomenon, it can only be identified as it crossed a boundary

between multiple systems that have different temperature to achieve equilibrium (Escudier & Atkins, 2019).

From a mathematical perspective, heat Q is understood as a manifestation of internal energy where in a medium with specific heat capacity c, density ρ, at temperature T, reside in a region R, $Q = \iiint_R \rho c T \, dV$. In that it is energy, with the unit joule J. Here, heat is defined as a manifestation of internal energy distributed throughout a medium.(Earl & Nicholson, 2021). Heat here is framed as an internal state function. The region R must be well defined, and the variables must be sufficiently continuous. Since the thermal equilibrium assumption need to be implemented, each differential volume element must be small enough to assume a uniform temperature. Mass density ρ relates spatial volume to matter content, specific heat capacity c encodes the proportionality between temperature and internal energy, temperature T represent the state variable capturing thermal intensity, and spatial domain R is bounded region within which the energy is considered. This formulation provides a bridge between microscopic thermodynamics and macroscopic energy accounting.

Internal energy U is defined as the total of kinetic energy of the atoms and molecules in a system and the potential energy of their mutual interactions. It is not energy of the whole system itself, hence doesn't include nuclear and inter-atomic/extra-molecular energies. Absolute value of the internal energy can't be measured directly. The focus for this subject is on the change of the energy ΔU (Rennie & Law, 2019).

Thermodynamics discussion requires a clear distinction between the term heat Q and internal energy U. According to the first law of thermodynamics, they relate within a system by the definition of a change in internal energy $\Delta U = Q - W$ where Q is energy interaction as heat occurring into the system and W is work done by the system on its surroundings. Heat is a path-dependent process and not a state function. An accurate approach to describe heat is in a standard molar (with unit kJ mol^{-1}) enthalpy change for the process under consideration. (Rennie & Law, 2019).

The temperature T(x,t) in a uniform solid medium, as governed by the heat equation, satisfies the parabolic partial differential equation $\frac{\partial T}{\partial t} = k \frac{\partial^2 T}{\partial x^2}$, where k

represents the thermal diffusivity of the medium (Earl & Nicholson, 2021). This is a reduced form of conservative of energy law under a specific assumption of homogeneity (the quality or state of being all the same or all of the same kind), no internal heat generation, and constant thermal diffusivity k. This is only applicable for heat transfer that only occur via conduction. The validity and integrity of this heat equation depends on the invariants of Fourier's Law (heat flux is proportional to the negative gradient of temperature, $q = -k\nabla T$), energy conservation, and linearity (non-linear cases like turbulent flows, radiation dominance will break the model). The spatial Laplacian $\frac{\partial^2 T}{\partial x^2}$ encodes spatial curvature of temperature, determining how heat "flows" from hotter to colder regions with its neighbouring environment. This provides a predictive model for how heat diffuses through solids. The structure shows that thermal evolution is irreversible and dissipative, which describe the Second Law of Thermodynamics

Physically, heat transfer is the transfer of energy between multiple systems because of difference in temperature (Rennie & Law, 2019). In the sense of mechanical engineering, heat transfer (also known as heat transport, heat transmission, and heat flow) is the transport of energy within or between object or fluid. There are 3 basic modes of the transportation: conduction, convection, and radiation (Escudier & Atkins, 2019).

In conclusion, heat transfer is the process by which energy moves across system boundaries due to temperature differences, acting as a path-dependent interaction that alters a system's internal energy, occurring only when crossing between systems and manifested through conduction, convection, or radiation, as shown in Figure 1.

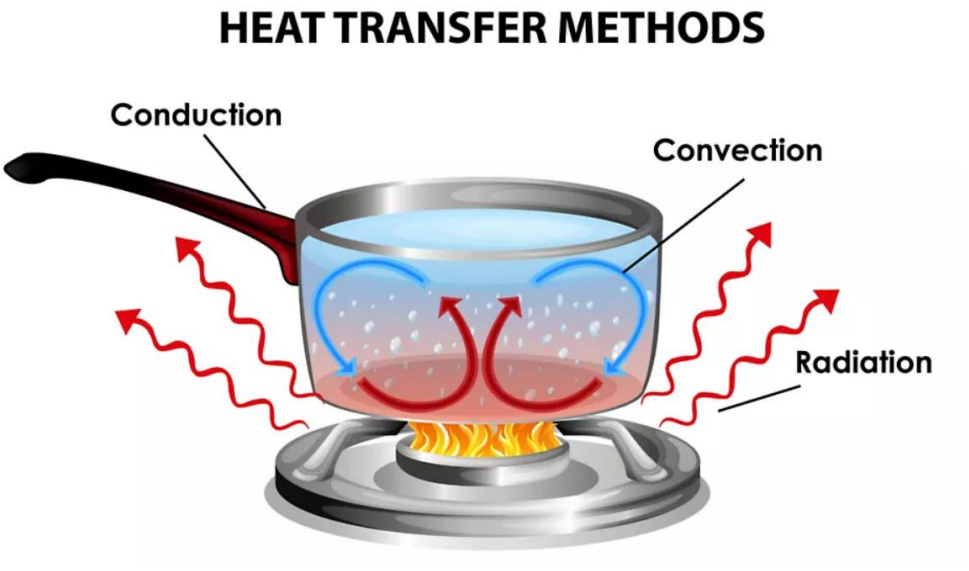

Figure 1: Heat transfer methods

1.2.1 Thermal Radiation

Radiation is energy travelling in the form of electromagnetic waves or photons (Rennie & Law, 2019). It refers to the electromagnetic energy emitted by a body because of its temperature, representing the conversion of internal energy into radiative energy. It shares the same physical nature as visible light, X-rays, and radio waves, differing only in wavelength and the mechanisms by which it is generated. All heated solids and liquids, and certain gases, emit thermal radiation. Radiative heat transfer occurs without any medium and, in fact, reaches its highest efficiency in a vacuum (Rohsenow et al., 1998).

1.2.2 Thermal Convection

Convection is process by which heat is transferred through the fluid itself. Natural convection is defined by the movement due to gravity; the hot part of the fluid expands, becomes less dense, and is displaced by the colder denser part of the fluid as this drops below it. This is the process that occurs in most domestic hot water. In some modern systems, where small-bore pipes are used or it is inconvenient to place the cylinder above the boiler, the circulation between boiler and hot-water cylinder relies

upon a pump. This is an example of forced convection, where hot fluid is transferred from one region to another by a pump or fan (Rennie & Law, 2019).

1.2.3 Thermal Conduction

Thermal conduction is the transmission of heat through a substance. In gases and most liquids, the energy is transmitted mainly by collisions between atoms and molecules with those possessing lower kinetic energy. In solid and liquid metals, heat conduction is predominantly by migration of fast-moving electrons, followed by collisions between these electrons and ions. In solid insulators the absence of free electrons restricts heat transfer to the vibrations of atoms and molecules within crystal lattices (Rennie & Law, 2019).

1.3 Hybrid Nanofluid

There are 2 states of motion studied in fluid mechanics which is statics and dynamics. Fluid statics is concerned with forces and pressures applied on idle liquids and gases while fluid dynamics study this condition on the fluid at motions (hydrodynamics for liquids, aerodynamics for gases)(Rennie & Law, 2019).

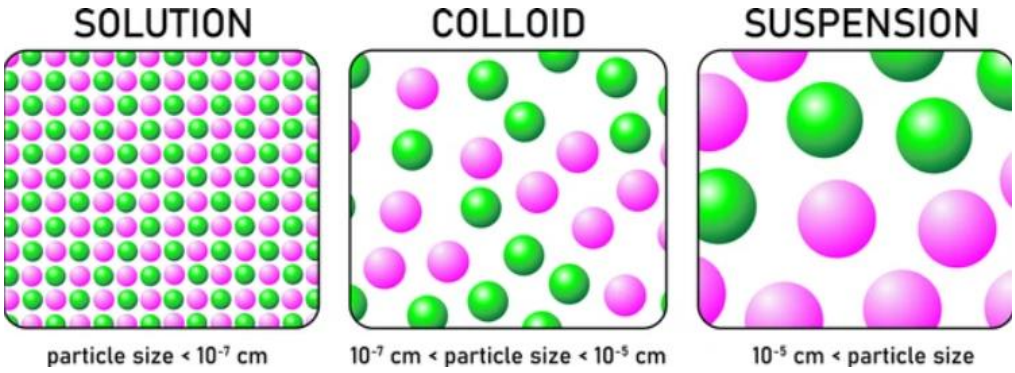

Figure 2: Colloidal Suspension of Nanoparticles

When a fluid flowing in medium with dimensions below 100nm, it is called nanofluidic, while nanofluid represent a colloidal suspension of nanoparticles in a base liquid (Escudier & Atkins, 2019) as shown in Figure 2. It is widely proven that nanofluids significantly improve thermal conductivity performance. Earlier studies show that this is the case due to the improvement in heat transmission capabilities.

This interest cause researchers to further the study on this matter with the exploration on dispersing multiple types of nanoparticles, hence the creation of "hybrid nanofluid". The unique properties of different nanoparticles interact synergistically, enhancing heat transfer performance by complementing each other's functions and compensating for individual limitations (Jusoh et al., 2024; Zainal et al., 2024). As hybrid composite is a composite reinforced by two or more variety of filament (Escudier & Atkins, 2019), hybrid nanofluid is saturation of more than one type of nanofluid. A single nanofluid is called mono nanofluid, while hybrid nanofluid could be ternary (trihybrid) nanofluid or beyond, even though it usually being used to refer to binary nanofluid up to this date.

In conclusion, hybrid nanofluid is a multiphase fluid formed by dispersing two or more types of nanoparticles into a base liquid at the nanoscale, resulting in a synergistic colloidal medium whose enhanced thermal performance arises from the combined interaction of distinct particle properties, thereby improving energy interaction under fluid motion.

1.4 Non-Newtonian Fluid

A Newtonian fluid is characterized by a linear relationship between shear stress and the velocity gradient, $\frac{F}{A} = \mu \frac{v}{d}$ where μ is the constant of proportionality (Newtonian viscosity). Hence, A non-Newtonian fluid is a fluid in which the relationship between shear stress and the velocity gradient does not consistently obey the linear model defined by Newton's law of viscosity. The viscosity is not constant and may vary with shear rate, time, or stress conditions. This type of fluid could exhibit increase in viscosity as the velocity gradient increases (dilatant during phenomenal dilatancy) like in some pastes and suspensions. There is no general theory has been developed to comprehensively describe them. However, it is common for non-Newtonian fluid to exhibit thixotropy where the viscosity depends on both velocity gradients and the time for which it has been applied (The faster a thixotropic liquid move, the less viscous it becomes) (Law & Rennie, 2020; Rennie & Law, 2019). Non-Newtonian fluid usually involving multiple combination of effects such as dependence of apparent viscosity

(effective viscosity, μ) on shear rate ($\dot{\gamma}$), normal stress (τ) in shear flow, time dependency, and memory effects (Escudier & Atkins, 2019). Because of these many kinds of rheological features different dependencies relational profile for different type and condition of non-Newtonian fluid, the behaviour for any non-Newtonian fluid can only be describes by using constitutive equations, an algebraic and numerical relation for the dependencies such as Hooke's Law, Newton's Viscosity Law, Fourier's Law, Fick's Law, and etc (Aminuddin, 2024; Escudier & Atkins, 2019).

One of the models used to study the behaviour of non-Newtonian fluid flow is the Powell–Eyring model. This model is known for its realistic consideration of shear-thinning behaviour in fluid viscosity. The constitutive equation is given by $T = \mu\nabla V + \frac{1}{\beta}\sinh^{-1}\left(\frac{1}{c}\nabla V\right)$ where μ is the dynamic viscosity, β and c are the characteristics of the Powell-Eyring model (Zaman et al., 2013), the material constants characterizing non-Newtonian response. The Powell-Eyring model is a constitutive equation describing the stress-strain relationship in non-Newtonian fluids that exhibits shear-thinning (viscosity decreases with shear rate). It is the extension of Newton's law of viscosity ($T = \mu V$, which assumes constant viscosity regardless of shear rate). The modal is applicable for fluid that exhibits shear-thinning behaviour, stable temperature and pressure, and the deformation rate is within a range where the inverse hyperbolic sine term realistically approximates molecular behaviour (if the deformation rate too low, the fluid looks nearly Newtonian with linear stress-strain, and if it too high, the molecular behaviour deviates beyond the validity of the Powell-Eyring model). To maintain the coherence of this model, the positivity of viscosity must hold, the material constants β and c must be realistic and calibrated experimentally, dimensional consistency, and the asymptotic limits (small and large shear rates) must agree with realistic observed fluid behaviour. The dynamic viscosity μ is for the baseline of Newtonian response, shear rate V is the driving variable controlling the stress, the material constants β and c shape the degree and onset of shear-thinning, the non-linear adjustment term $\frac{1}{\beta}\sinh^{-1}\left(\frac{1}{c}\nabla V\right)$ capture the departure from Newtonian linearity. This formulation describe a smooth transition between Newtonian behavior at

low shear rates and strong non-Newtonian effects at high shear rates. If $\mu = 0$, only the non-linear term remains; at very low shear, the model loses Newtonian recovery and fails. If β and c are mis-specified, predictions deviate drastically, especially in high-shear conditions.

In conclusion, a non-Newtonian hybrid nanofluid is a colloidal suspension of two or more distinct nanoparticles in a base fluid that exhibits spacetime-dependent or complex rheological behaviour such as shear-thinning, shear-thickening, or thixotropy deviating from Newton's law of viscosity. One of its key advantages is leveraging synergistic nanoparticle interactions to enhance thermal performance beyond that of mono nanofluids.

1.5 Boundary Layer

Boundary layer is a thin layer of fluid formed on the surface relative to which the fluid is flowing. When a fluid touches a surface during the flow, it causes an adhesion between the molecules of the fluid closest to the solid surface result to those molecules of the fluid to be relatively stationary. The velocity of the fluid reduces from the value of free flow, U_∞ approaches to 0 relative to its closeness to the solid surface because of the attraction force between the molecules is stronger here. This is what we called as no-slip boundary condition, an accurate assumption for approximation for macroscopic flow, but not accurate at molecular scale. The opposition assumption for this boundary slip is slip boundary condition. This is the phenomena where viscosity in the bulk and at the surface of the liquid to be different (Asshaari & Md Jedi, 2022; Rennie & Law, 2019). The effect of viscosity is a key here. The Navier-Stokes equations are used to analyse the boundary layer, where the height of the layer approached to 0, and the effect of viscosity are approached to 0 at outside of the boundary layer (Earl & Nicholson, 2021).

In a field of mechanical engineering, there are two main topics on the boundary layer, the hydrodynamic boundary layer (velocity) and the thermal boundary layer (temperature). Hydrodynamic boundary layer is a developing region within a fluid that caused by the viscosity of the fluid when it flows over a surface. A stationary molecule

of the fluid closest to the surface approaches to its free-stream value at the border of the boundary layer. Reynold number is used to identify the type of flow within the boundary layer whether it is laminar, transitional or turbulent. The thermal boundary layer is the thin region of a fluid near surface where heat transfer occurs due to a temperature difference between the surface and the free stream, resulting in a temperature gradient within the fluid (Escudier & Atkins, 2019). It is mentioned by Asshaari & Md Jedi (2022) that the temperature differences also occur due to the velocity of the fluid flow where the gap in temperature increase as the velocity of the fluid increase. This gap in temperature is also what we call thermal boundary layer. There is also research on the third kind of boundary layer which is concentration boundary layer (Asshaari & Md Jedi, 2022) where the boundary is defined by the difference in the concentration of the fluid.

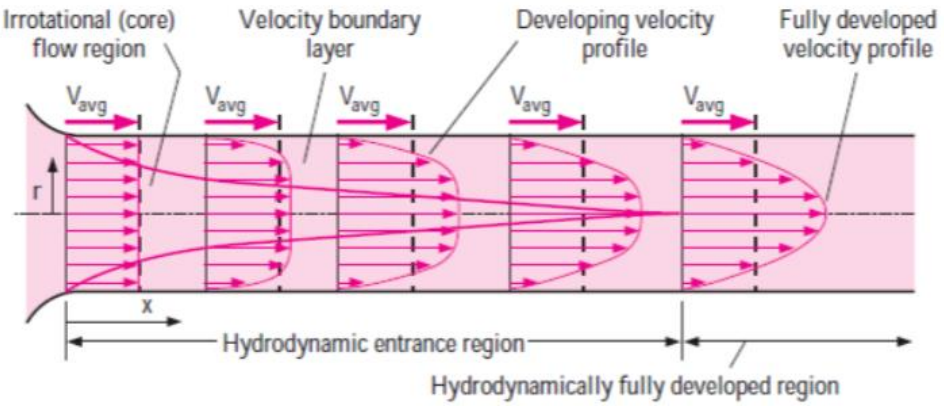

Figure 3: Boundary layer flow in pipe

Figure 3 illustrates the formation of a boundary layer within a pipe, where the fluid velocity transitions from zero at the wall (due to the no-slip condition) to the free-stream value at the pipe's centre. This gradient arises from viscous shear forces that dominate near the solid surface. The hydrodynamic boundary layer represents the velocity profile development, while the accompanying thermal boundary layer shows how temperature decreases from the heated wall toward the core fluid. The figure emphasizes how viscous and thermal effects confine most changes in velocity and temperature to a thin region adjacent to the wall, a key feature in analysing Powell-Eyring hybrid nanofluid flow under magnetohydrodynamic and radiative influences

inside conduits, where understanding these gradients is essential for predicting heat-transfer performance.

In conclusion, boundary layer is the region of a fluid flow adjacent to a solid surface where the effects of viscosity are significant, resulting in steep gradients of physical properties such as velocity, temperature, or concentration, due to the no-slip condition or thermal interaction at the surface, regardless of the region's geometric thickness.

1.6 Problem Statement

Hybrid nanofluids (HNFs) are known to enhance thermal conductivity. However, most researchers adopt a narrowly focused scope, despite the wide range of non-Newtonian fluid behaviours that could be considered for specific applications. Very few studies couple Powell-Eyring shear-thinning rheology with the simultaneous action of magnetohydrodynamics, Joule heating, non-linear thermal radiation and Newtonian surface heating in a unified boundary-layer framework for application in solar collector devices. Even the latest tri-hybrid investigations still exclude key loss mechanisms. It is required for a rigorously validated, integrated model that captures these concurrent effects over the receiver surfaces found in the renewable-energy hardware.

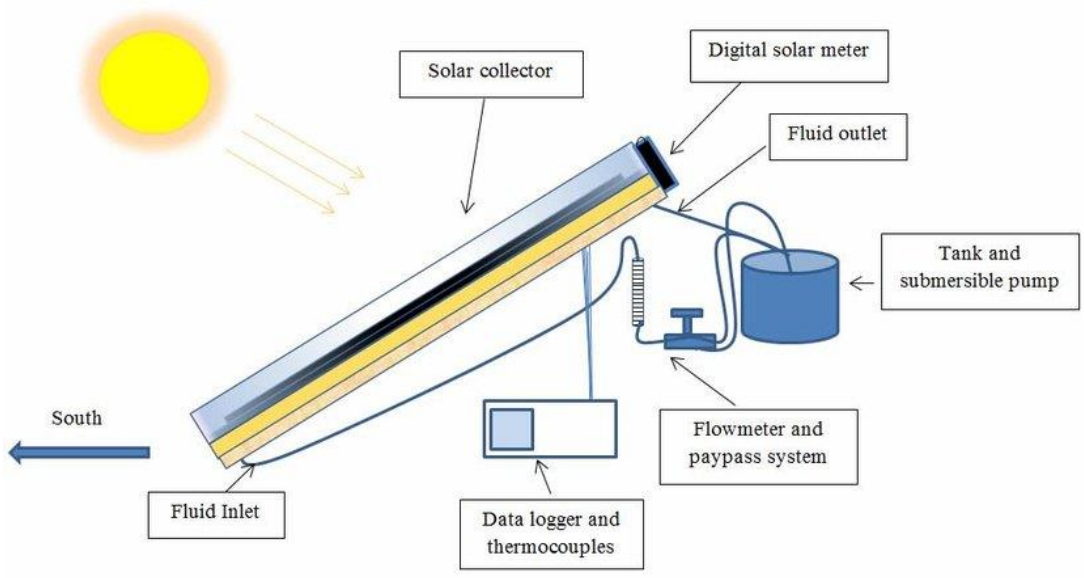

Figure 4: The Schematic of Flat Solar Collector

Figure 4 presents the basic working principle of a flat-plate solar collector, the central system motivating this study. Solar radiation passes through a transparent cover and strikes the absorber plate, where heat is transferred to a working fluid flowing beneath it. However, in conventional systems, the low thermal conductivity of standard fluids like water or ethylene glycol limits the rate of heat absorption and transport. This inefficiency leads to energy losses and reduced collector performance. The figure thus highlights the key physical domain of the research problem: improving the heat-transfer mechanism within the absorber channel

Existing studies on hybrid nanofluid heat transfer often neglect the combined effects of Powell-Eyring non-Newtonian rheology, magnetohydrodynamics, Joule heating, non-linear radiation, and Newtonian wall heating, resulting in incomplete predictive models for real solar collector surfaces. Moreover, the Powell-Eyring model offers a more realistic representation of such non-Newtonian flows, yet it remains underexplored in hybrid nanofluid applications. Furthermore, while MATLAB's bvp4c solver is widely accepted for boundary-layer problems, this study introduces the backward differentiation formula (BDF) as a relevant alternative approach, aiming to improve the handling of stiff and highly non-linear equations and to broaden the numerical framework for future modelling of advanced thermal systems.

Runge-Kutta and MATLAB bvp4c are widely used, but their mesh adaptation deteriorates for strongly non-linear, stiff ODE systems that arise when MHD forces and viscous dissipation are large. backward differentiation formula (BDF) offers better stability and has not been benchmarked against bvp5c for Powell-Eyring HNFs. Consequently, the community lacks solver reliability guidelines for collector-design calculations.

1.7 Research Objectives

1. To formulate mathematical models of Powell-Eyring hybrid nanofluid flow with thermal radiation over various plate orientation, and porous medium accounting for magnetohydrodynamics (MHD), and Joule heating effects under a steady and unsteady condition.

2. To transform the governing models into a system of ordinary differential equations (ODEs) through appropriate similarity variables.
3. To solve the resulting equations numerically using backward differentiation formula (BDF) and MATLAB's solver.
4. To analyse the impact of thermal radiation, MHD, Joule heating, and Newtonian heating on the behaviour of the fluid flow and heat transfer.

1.8 Research Questions

1. How can the Powell-Eyring model be applied to accurately describe the non-Newtonian behaviour of hybrid nanofluid flows under combined effects of magnetohydrodynamics, Joule heating, thermal radiation, and Newtonian wall heating?
2. What are the governing equations and similarity transformations that best represent these coupled physical phenomena over various surface orientations and porous media?
3. How does the backward differentiation formula (BDF) compare with MATLAB's bvp5c solver in terms of efficiency, convergence, and suitability for stiff and highly non-linear boundary-layer problems?
4. In what ways do parameters such as magnetic field strength, thermal radiation, and nanoparticle concentration influence velocity, temperature distribution, skin friction, and Nusselt number within the hybrid nanofluid flow?

1.9 Significance of Study

This research carries meaningful benefits across multiple areas of life. For society, it supports the global shift toward cleaner and more sustainable energy. By improving how we transfer and manage heat in solar energy systems, the study helps make renewable technologies like flat plate and parabolic trough solar collectors more efficient and practical for everyday use. This means better access to affordable and eco-friendly energy for households and communities, especially in regions with high solar potential.

In the world of academia, the study brings fresh insights by combining several advanced concepts like non-Newtonian fluid behaviour, hybrid nanofluids, and magnetic and thermal effects, into one unified mathematical model. Using the Powell-Eyring model and advanced numerical methods like the backward differentiation formula (BDF), it opens new pathways for researchers to study complex heat flow systems more accurately. This contribution helps push the boundaries of applied mathematics and fluid dynamics research.

For government and policymakers, the research offers data and tools that can be used to set better design standards and performance expectations for renewable energy infrastructure. With more reliable modelling, solar systems can be built to perform better under real-world conditions, supporting national energy goals and long-term climate commitments.

From an industry point of view, especially in the energy and engineering sectors, the findings can guide manufacturers and designers in improving the performance of solar collectors. Better thermal fluids mean better energy capture and lower energy losses, translating into more cost-effective and high-performance systems for consumers and businesses alike.

Lastly, when we look at the environment, this study supports efforts to reduce our dependence on fossil fuels. By boosting the efficiency of solar thermal systems, we can produce more energy with less environmental impact. That means lower carbon emissions, less pollution, and a step forward in protecting our planet for future generations.

1.10 Scope and Limitation

This research is limited to two-dimensional, laminar boundary-layer flow of a Powell-Eyring hybrid nanofluid past an infinite flat plate is modelled. The plate may be vertical, horizontal or inclined. Using A binary Cu-Al_2O_3/EG hybrid nanofluid is treated as a single-phase homogeneous mixture. The momentum-energy system incorporates MHD, thermal radiation, Joule heating, Newtonian heating. Boundary-layer and

similarity approximations reduce the PDE set to coupled, high-order ODEs. To validate the results, the ODEs will be solved using backward differentiation formula (BDF) and MATLAB's bvp5c solver. Outputs include skin-friction coefficient C_xf, local Nusselt number Nu_x,

CHAPTER 2
LITERATURE REVIEW

2.1 Boundary layer flow of Powell-Eyring Model

Non-Newtonian fluids show distinct rheological behaviour that can be advantageous in thermal conductivity and heat transfer. The Casson model is frequently used to describe the behaviour of non-Newtonian hybrid nanofluids. There is also other more frequently used model like Carreau-Yasuda model and the Reiner-Philippoff model (Alrashdi, 2023; Mohamad et al., 2024). However, it is very few research that use Powell-Eyring model.

In an article by Alrashdi (2023), it is written that he uses Carreau-Yasuda model as her base model on the non-Newtonian rheological properties to study the behaviour of graphene nano-powder and ethylene glycol during peristalsis. Rashad et al. (2023) introduced the Powell-Eyring non-Newtonian model into a hybrid nanofluid context. They investigate mixed convection flow of a Powell-Eyring hybrid nanofluid past a vertical plate embedded in a porous medium, including thermal radiation and internal heat generation. They use Cu-Fe_3O_4/EG as the hybrid nanofluid. The study is notable for combining magnetic field, thermal radiation, porous media, and a non-Newtonian (Powell-Eyring) hybrid nanofluid. They solved the non-similar boundary-layer equations using a hybrid scheme: local non-similarity with RKF45 with shooting. The main finding is increasing magnetic field (Hartmann number) implies reduced velocity, drag changes, and overall decrease in heat transfer rate (Nusselt number), and increasing thermal radiation and heat generation cause raised wall temperature and increased Nusselt number (heat transfer). The model has a kinetic-theory basis and reduces to Newtonian behaviour at shear extremes, overcoming shortcomings of power-law and Spriggs models

The critical insights from Nabwey et al. (2023) reveal that among various non-Newtonian fluid models, the Powell-Eyring model holds a distinctive position, representing only about 5% of the studies surveyed by Nabwey et al.. This indicates that relatively few research papers have focused on it. This scarcity is reasonable, since the

Powell-Eyring model uniquely bridges kinetic theory and continuum mechanics, capturing both shear-thinning and shear-thickening behaviours without the singularities found in power-law or Casson models. Within the comparative framework of non-Newtonian nanofluid models, the Powell-Eyring formulation stands out as a versatile rheological representation for thermal-fluid analysis, capable of reducing to Newtonian behaviour at both high and low shear rates while preserving nonlinearity in intermediate regimes. This characteristic makes it highly suitable for boundary-layer flow studies involving magnetohydrodynamic (MHD) and Joule-heating effects, where velocity gradients and internal heat generation vary significantly. A study by Challa et al. (2025) explores how Powell-Eyring nanofluid behaves as it flows over an unsteady stretching surface under the effects of Stefan injection or suction. The study shows that as the Brownian motion parameter increases; the fluid's temperature rises while the concentration of nanoparticles decreases. Additionally, an increase in the magnetic number leads to a reduction in the velocity profile.

2.2 Boundary Layer Flow in Nanofluid

Researchers generally agree that the size, shape, and material of nanoparticles play a significant role in determining the thermal and rheological properties of hybrid nanofluids. Smaller nanoparticles tend to provide better thermal conductivity, while the shape can influence flow behaviour and stability. Furthermore, hybrid nanofluids (HNFs) generally have a better thermal conductivity and heat transfer capabilities compared to traditional fluids and mono nanofluids. The idea starts emerging in 2010s, such as Suresh et al. (2012) and Madhesh & Kalaiselvam (2014), in an experimental work to enhance further the heat transfer capability in non-Newtonian fluids, nanofluids, by implementing hybrid between two nanofluids, Alumina (Al_2O_3) and Copper (Cu). The combination of different nanoparticles, such as Cu and Al_2O_3, in a base fluid like water or ethylene glycol, enhances the thermal performance significantly.

Research on the shape of nanoparticle effect the rheology of nanofluids has been conducted by Tabassum & Mehmood (2020) where they found out that surface shear stress increases with the viscosity variation parameter but decreases as the material constant rises. Among the tested types, blade-shaped nanoparticles show the highest effectiveness in enhancing heat transfer in this scenario. Adun et al. (2021) showed that

smaller nanoparticles improve thermal conductivity more efficiently. Arguably that their larger surface area allows better heat transfer.

Different studies highlight various combinations like Cu-Al_2O_3, Fe_3O_4-MWCNT (Multi-walled Carbon Nanotubes), and ZnO-Al_2O_3-SiO_2, each showing unique advantages. The debate continues the best nanoparticle volume fractions and their impact on thermal efficiency and friction factors. Saleh & Sundar (2021) found that Fe_3O_4-MWCNT hybrid nanofluids demonstrated a 28.46% increase in thermal conductivity and a 39.22% increase in the heat transfer coefficient at a 0.3% volume concentration. The optimal volume fraction for maximum thermal efficiency was 0.3%, balancing thermal conductivity and friction factor. One of the primary challenges in the application of hybrid nanofluids is their stability. One of the solutions for this is as proposed by Mane & Hemadri (2022), where surfactants can greatly enhance the stability of nanofluids by preventing nanoparticle agglomeration. However, it still requires further research into more methods to enhance the stability of these fluids.

Nabwey et al. (2023) have concluded in their critical literature review that Al_2O_3 is more efficient in term of thermal conductivity for heat transfer compared to another nanoparticle and CuO is the second most encountered nanoparticle used. While water and carboxy methyl cellulose (CMC) is the most investigated base fluid, Ethylene Glycol (EG) only contributes to 5% of the total research papers. Therefore, this research will use Al_2O_3-Cu/EG as the fluid for the heat transfer studies. The chosen hybrid nanoparticles and base fluid expected to reduce the agglomeration problem, as nanoparticles tend to agglomerate, which can significantly affect the thermal properties and efficiency of the nanofluids because of attraction between particles, arguably by reducing the thermal conductivity and increase the viscosity (Manimaran et al., 2025).

2.3 Boundary Layer Flow with Various Orientations

The inclination of the plate relative to the gravitational vector modifies the buoyancy forces and pressure distribution in convective flows. For a heated plate in air, gravity induces a buoyant force that drives natural convection along the plate. If the plate is vertical (inclination angle 0 degree from vertical), the buoyancy force acts fully in the direction of the plate, maximizing the aiding convective flow. If the plate is tilted

toward horizontal (90 degree from vertical), the component of gravity along the plate is reduced (and at exactly horizontal, buoyancy acts upward perpendicular to the plate, not driving flow along it). Thus, increasing the inclination angle (toward horizontal) generally dampens the buoyant flow along the surface. As the plate becomes less vertical, the driving force for free convection decreases, causing lower fluid velocities along the plate and a thinner momentum boundary layer. At the same time, reduced convective motion means heat builds up more in the fluid near the plate, enhancing the thermal boundary layer. It is important to note how inclination is defined; many researchers measure the angle α from the vertical. In that convention $\alpha = 0$ is vertical and $\alpha = 90°$ is horizontal; an increase in α reduces buoyancy-induced acceleration along the plate. (Some works use the complementary definition from horizontal, which can invert the described trend if not noted.) Aside from buoyancy, inclination can also affect pressure gradients in forced flows (e.g. an inclined stagnation flow will have a component of dynamic pressure along gravity), and it influences the tendency for flow separation in external flows. In inclined free convection, as α approaches 90°, the flow can transition toward a pure horizontal plate scenario where a stable thermal stratification forms above the plate rather than a strong upslope current.

Hayat et al. (2014) demonstrate this effect, when an inclined stretching sheet's angle is raised from vertical toward horizontal, the flow decelerates and the fluid temperature rises, because buoyancy forces diminish with inclination. Inclination also matters for stability and dual solutions. Anuar et al. (2021) studies Ag-MgO/water hybrid nanofluid flow on an inclined stretching/shrinking sheet with buoyancy (mixed convection) effects. They explicitly include an inclination angle parameter (α) in the governing equations with buoyancy model through the parameter λ, distinguishing assisting ($\lambda > 0$) and opposing ($\lambda < 0$) flows. The study shows that increasing inclination enhances buoyancy, which increases heat transfer (Nusselt number) and skin friction under certain conditions. They found dual branches (stable first solution, unstable second), consistent with boundary-layer separation dynamics. Aljabali et al. (2025) also confirm the general trends the as the inclination angle increases, the $\cos(\alpha)$ terms reduce the buoyancy effect, which in turn affects heat transfer depending on whether the flow is assisting or opposing.

Overall, plate inclination provides a means to tune the relative influence of buoyant forces, with vertical plates promoting stronger convection currents and horizontal plates relying more on pure conduction unless other forcing is present.

2.4 Thermal Radiation

Early foundational work on non-Newtonian radiative transport began with Hayat et al. (2014), who analysed the unsteady Powell-Eyring fluid past an inclined stretching sheet with non-uniform heat source and sink under the influence of thermal radiation. Their study revealed that radiative flux enhances both the thermal boundary layer thickness and surface Nusselt number, establishing the groundwork for coupling radiative and non-Newtonian effects in time-dependent stretching flows. Subsequently, Krishna et al. (2016) extended this idea by incorporating chemical reaction, suction, and injection in an unsteady Powell-Eyring fluid past an inclined stretching sheet. Their investigation shows that radiation parameter depreciates heat transfer rate while enhancing the temperature distribution with the increase of mass transfer rate, implying that excessive radiative absorption thickens the thermal layer. Together, these two early contributions confirmed that radiative heat transport must be explicitly modelled in Powell-Eyring boundary layer systems due to its nonlinear influence on energy gradients.

In more complex three-dimensional configurations, Muhammad et al. (2021) analysed nonlinear thermal radiation in Powell-Eyring nanofluid flow with Arrhenius activation energy. They observed improvement of radiation parameter cause the increase of volume friction, while the temperature distribution decreases with relaxation heat diffusion. According to M. S. Khan et al. (2021), when non-linear thermal radiation becomes more significant, it helps boost heat transfer within the fluid, leading to a higher overall temperature. However, the effects of non-linear radiation on hybrid nanofluid flows are not fully understood and require further investigation. Understanding these effects can lead to better optimization of heat transfer systems in solar collectors and other applications.

2.5 Magnetohydrodynamics Effect

The application of magnetic fields in MHD flows of hybrid nanofluids can control and enhance heat transfer rates. Magnetic parameters generally reduce velocity profiles but increase temperature profiles, contributing to better thermal management. An increased magnetic field parameter generally reduces the velocity profile due to the Lorentz force but increases the temperature profile through enhanced heat transfer.

Khan et al. (2015) find out that steady Powell-Eyring flow shows Joule heating (via the Eckert number) and thermal radiation significantly raise the fluid temperature, which is critical in modelling heat transfer in MHD flows. It also confirms that MHD (magnetic field) induces Lorentz forces, which reduce velocity but enhance thermal profiles, behaviours essential for flat plate thermal boundary layers in Powell-Eyring fluid systems. In a study by Saleh & Sundar (2021) involving a radially stretching sheet, the magnetic field reduced velocity but increased temperature due to the Lorentz force. The research by Naseem et al. (2023) also concludes with the same outcomes.

Although a study by Bibi et al. (2023) looks at a Newtonian fluid, its findings give valuable insight to compare with Powell-Eyring flows. It shows that when thermal diffusion (Soret effect) and viscous heating (Eckert number) increase, the fluid's velocity and temperature also rise. At the same time, a stronger magnetic field slows the flow, something we also expect in Powell-Eyring models. These results help us understand how MHD and heat-related effects could influence more complex, non-Newtonian flows over a flat plate with thermal radiation. Norzawary et al. (2023) shows two nanoparticles give improved heat transfer over single cases, at the cost of higher skin friction. It confirms dual solutions with suction stabilizing the first branch. The study importantly strengthens the numerical approach and provides baseline comparisons that later MHD and radiative studies can build upon.

By performing research on unsteady inclined magnetohydrodynamic (MHD) Powell-Eyring fluid with microorganisms, Parmar et al. (2024) find out that there is a direct relationship in which the increase in heat generation and non-linear radiation lead to higher temperature distribution. Maiti & Mukhopadhyay (2025) demonstrated that

Newtonian heating significantly enhances temperature distribution in Powell-Eyring fluids by strengthening surface-to-fluid heat transfer.

There is a need for more comprehensive models that integrate various physical phenomena such as magnetohydrodynamics, porosity, thermal radiation, and heat generation/absorption in hybrid nanofluid systems for specific application. Current models often lack the ability to predict the behaviour of these complex systems accurately.

2.6 Porous Medium

Porous media serve as an essential framework in modern heat-transfer studies due to their ability to enhance thermal performance through interstitial flow between solid matrices and voids. Zaman et al. (2013) provided a complementary theoretical perspective by studying unsteady incompressible Couette flow of a Powell-Eyring non-Newtonian fluid bounded by porous plates. Their analysis demonstrated how uniform suction and injection at the walls influence wall shear stress in time-dependent flow fields. The results reinforce the idea that the inclusion of porous structures not only affects the flow resistance but also introduces coupling between fluid rheology and wall permeability, conditions highly relevant to hybrid nanofluid flow under magnetohydrodynamic and Joule-heating environments envisioned in this research.

In a broader context, Badruddin & Quadir (2016) reviewed decades of work on heat transfer in porous domains with varied geometries such as vertical plates, cavities, and annuli. Their mini-review concluded that although porous-medium convection has been extensively explored, the porous medium usage in various geometrical shapes still unexplored. We can also identify the significant gaps remain in understanding the combined influence of radiation, viscous dissipation, and non-equilibrium effects on hybrid nanofluids. They highlighted that, while radiation enhances overall heat-transfer rates, conduction tends to dominate within the porous matrix, creating a non-linear interplay yet to be fully modelled.

Nabwey et al. (2023) presented a comprehensive review describing porous materials as heterogeneous structures whose porosity directly governs permeability and

heat-transport characteristics. Their analysis emphasized that porous matrices, when filled with nanofluids or hybrid nanofluids, substantially modify the overall heat-transfer rate by increasing the fluid displacement and heat conduction to solid surface. They demonstrated that macroporous structures (pore size > 50 nm) are especially suitable for nanofluid and hybrid-nanofluid applications because they allow nanoparticle-enhanced thermal conduction without hindering fluid motion by causing the nanoparticle to have a uniform distribution. In fact, they argue that nanofluids can in macroporous. Moreover, Nabwey et al. identified that Darcy's number and the porosity coefficient exert a direct proportional effect on the Nusselt number due to the increase of the volume friction of the fluid nanoparticles, revealing that any variation in permeability or void fraction linearly affects heat transfer in nanofluid-saturated porous systems.

In summary, all these research reaffirmed that despite substantial progress, the modelling of nanofluid and hybrid-nanofluid heat transfer in porous media remains incomplete, particularly when incorporating Powell-Eyring model of non-Newtonian rheology, magnetohydrodynamics, Joule heating and radiation effects. This unresolved complexity justifies the present study's focus on developing a Powell-Eyring hybrid-nanofluid model in porous media, providing a more accurate representation of multiphase energy transport for realistic engineering applications.

2.7 Joule Heating

Earlier studies provide a chronological development of the effect of Joule heating on the heat transfer through nanofluid. Abolbashari et al. (2014) conducted one of the pioneering analyses by examining entropy generation in an unsteady MHD nanofluid over a stretching permeable surface. Their work showed that the Joule dissipation irreversibility parameter occur with the increase of Brinkman number entropy production which increase the entropy generation due to the fluid friction, illustrating how electrical resistance within the fluid could raise internal energy and degrade thermal efficiencies. Building on this, N. A. Khan et al. (2015) incorporated thermophoresis and chemical reactions into a Powell-Eyring MHD flow and found that in the presence of thermophoresis, Joule heating and chemical reaction, the thermal radiation substantially effects velocity profile.

A further refinement was made by Hayat et al. (2016), who analysed Powell-Eyring flow under the combined effects of thermal radiation, Joule heating, and cross-diffusion phenomena, specifically Soret and Dufour effects. Their analytical solutions revealed that Joule heating elevated temperature profile and decrease the local Nusselt numbers. This study confirmed Joule heating acts as an internal heat source that thickens the thermal boundary layer and lowers wall heat transfer. Naseem et al. (2023) later explored Joule heating in a Powell-Eyring fluid with radiation and found that the Eckert number and magnetic parameter strongly amplify thermal boundary-layer thickness. Their results suggested that the temperature field is sensitive to Joule-induced internal heat generation, making it indispensable for accurately modelling heat transport in electrically conducting non-Newtonian flows.

In summary, Joule heating has evolved from being treated as a minor resistive effect to a central mechanism influencing temperature, entropy, and flow stability in MHD non-Newtonian nanofluids. The proposed study therefore aims to bridge this research gap by applying the Powell-Eyring hybrid nanofluid model to examine Joule heating effects in complex boundary-layer environments, an essential step toward optimizing energy transport in advanced thermal systems.

2.8 Numerical Method

Different numerical and computational methods are used to model hybrid nanofluid flows, including the Runge-Kutta method, Finite Difference-Control Volume Method, and Finite Element Method (FEM) (Majumdar, 2021). The choice of modelling approach can affect the result, leading to debates on the most accurate and reliable methods.

Finite difference methods (FDM) involve discretizing the differential equations on a mesh and solving the resulting algebraic system. They have been widely used in boundary-layer flow simulations, including Powell-Eyring fluid problems. A prominent FDM approach for steady boundary layers is the Keller-Box scheme, an implicit second-order accurate finite difference method known for its stability and fast convergence. For example, Jamshed et al. (2021) implemented the Keller-Box

technique to solve a Powell-Eyring nanofluid flow with MHD, radiation, Joule heating, etc., and reported that this implicit FDM is “convergent up to second order and inherently stable”, satisfying Von Neumann stability criteria.

Shampine et al. (2000) note that while bvp4c is an effective and convenient solver, its default algorithm “is not appropriate for high accuracies nor for problems with extremely sharp changes in their solutions”. Many researchers in this domain have leveraged bvp4c to obtain solutions for non-Newtonian nanofluid flows. For example, multiple theses and papers have reported using bvp4c to solve Powell-Eyring fluid models with radiation and other effects. In one comparative study, Muhammad et al. (2021), solved a 3D Powell-Eyring nanofluid flow with thermal slip and activation energy using both bvp4c and a shooting method, finding good agreement between the two approaches

The backward differentiation formula (BDF) is an implicit multistep method designed for solving stiff ordinary differential equations by generating multiple approximate solutions. In advancing the numerical modelling of complex fluid flows such as Powell-Eyring hybrid nanofluids, the backward differentiation formula (BDF) has emerged as a robust alternative to traditional finite difference and Runge-Kutta based solvers. Recent work by James Audu et al. (2022), introduced a two-step BDF scheme constructed through interpolation-collocation hybridization using power series basis functions, achieving a ninth-order convergent, zero-stable, and self-starting implicit solver for fourth-order differential systems. Their findings demonstrated that BDF yields superior precision and stability in both linear and nonlinear test problems compared to conventional hybrid block approach. Such characteristics make the BDF framework particularly suitable for the stiff and nonlinear coupled systems encountered in nanofluid dynamics and MHD flow modelling, where high-order accuracy and stability are critical for capturing strong gradients, boundary layer phenomena, and nonlinear heat transfer effects. Thus, implementing BDF alongside MATLAB’s bvp5c solver in this research offers not only methodological novelty but also a meaningful enhancement in numerical reliability and computational rigor.

The presence of strong MHD, viscous dissipation, and thermal radiation can make the ODE system stiff, meaning solutions may exhibit boundary layers or rapid

changes that are challenging for standard explicit solvers. Moreover, these equations are highly nonlinear and often do not admit closed-form solutions, so robust numerical methods are required. Backward differentiation formulas (BDF) are greatly useful for stiff ordinary differential equations (ODE). It is necessary to convert boundary value problem (BVP) into initial value problem (IVP) to implement this method. This paper will implement BDF with independent parameter on the entropy analysis of heat transfer in the hybrid nanofluid.

2.9 Conclusion

From the literature review, it shows that there are limited studies on Powell-Eyring hybrid nanofluids, especially for specific real-world application such as on inclined surface of flat solar collector. The engineering world needs comprehensive model which have MHD mixed convection flow of a Powell-Eyring hybrid nanofluid over an inclined plate with thermal radiation to be implemented in the renewable energy applications. By doing so, we can discover interactions that previous isolated studies could not. For example, how non-Newtonian viscosity might alter the optimal nanoparticle fraction or how it influences dual solution behaviour in inclined flows.

Furthermore, there is also lack of systematic comparison of numerical methods for these equations. Most of the studies typically uses one numerical method just to solve the equations, but this raise a question that there might be using a counter-productive numerical method for their application. Hence, it is possible that minor discrepancies between papers are due to numerical error or insufficient convergence. It is required for a further study on how to explain the discrepancies from numerical perspective in addition to the physical effects by the fluid itself.

This proposed research will address the current literature gaps by providing a unified, well-vetted analysis of MHD hybrid nanofluid flow on inclined surfaces using the Powell-Eyring model. It will clarify inconsistent results by enforcing consistent definitions and exploring the full parameter space, thereby contributing both to theory (better models and methods) and practice (clear guidelines for use of hybrid nanofluids in MHD convective cooling).

CHAPTER 3
RESEARCH METHODOLOGY

3.1 Research Framework

This study's methodology begins by deriving a physics-specific boundary-layer model for a Powell-Eyring hybrid nanofluid, embedding non-Newtonian shear-thinning rheology, dual-nanoparticle mixture rules, thermal radiation and magnetic forcing into the momentum-energy equations. The base fluid is ethylene glycol, EG and the suspended nanoparticles are Alumina-Copper Al_2O_3-Cu, forming a homogeneous mixture.

Figure 5 illustrates the structured research workflow adopted in this study, beginning with the formulation of mathematical models for Powell-Eyring hybrid nanofluid flows under varying conditions, including magnetohydrodynamics (MHD), thermal radiation, Joule heating, and Newtonian wall heating across different plate orientations. The framework demonstrates how each physical model is transformed from partial differential equations (PDEs) into ordinary differential equations (ODEs) through similarity transformations, preparing them for numerical computation.

Two complementary solvers are then employed: MATLAB's bvp5c, a fifth-order collocation method, and the backward differentiation formula (BDF), chosen for its superior stability in stiff, highly non-linear systems. Their parallel use allows systematic validation and benchmarking, reinforcing the numerical reliability and novelty of the approach. The framework concludes with performance evaluation, comparing results for skin friction, Nusselt number, and flow behaviour, to determine the optimal configuration for enhanced heat transfer in renewable-energy systems like flat-plate solar collectors.

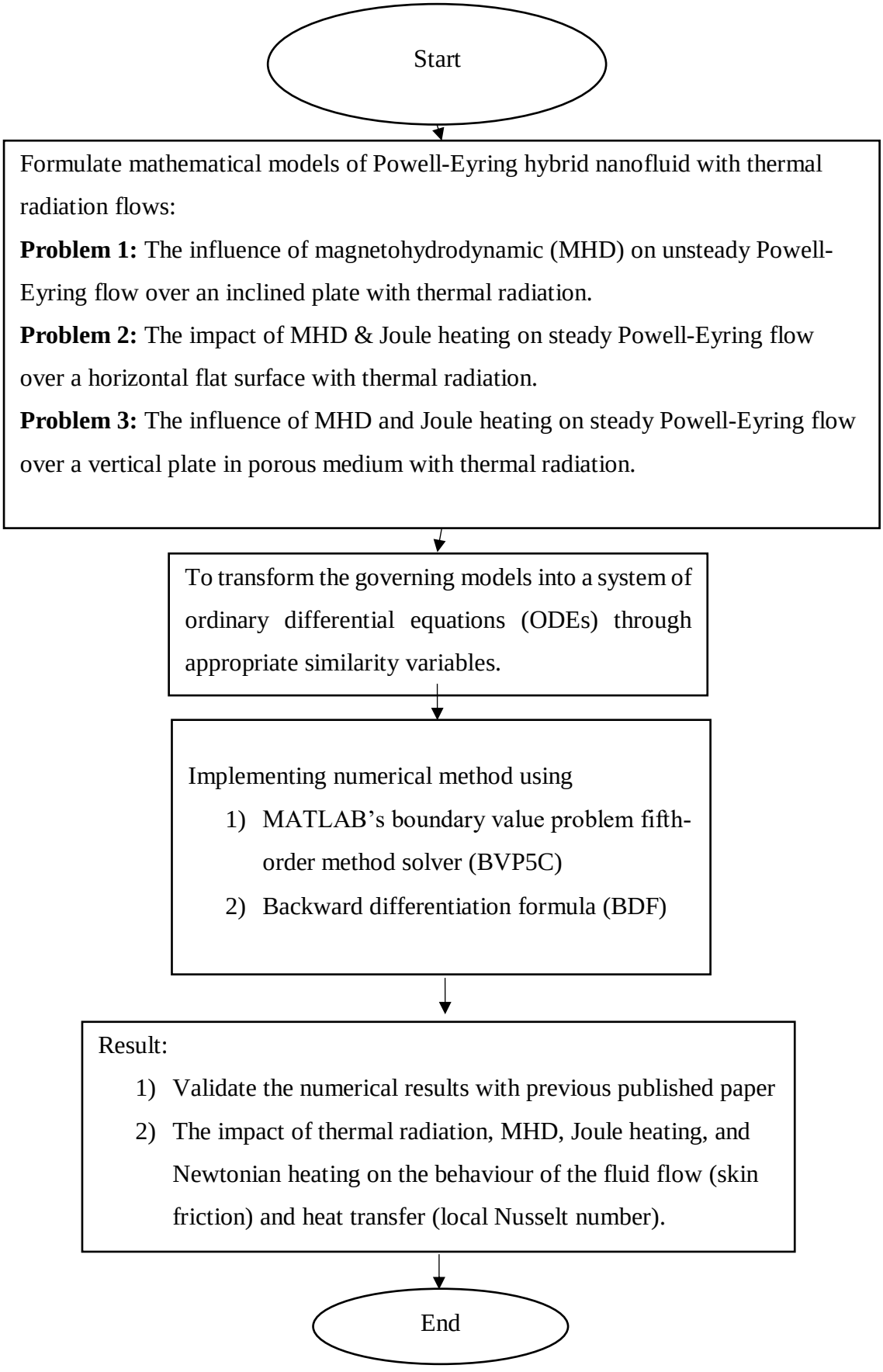

Figure 5: Research Framework

3.1.1 Problem 1: The influence of magnetohydrodynamic (MHD) on unsteady Powell-Eyring flow over an inclined plate with thermal radiation.

For this problem, a two-dimensional (2D), incompressible, laminar and homogeneous mixture is considered, where the thermophysical properties follow the Maxwell-Garnett and Brinkman models. The study involves an unsteady boundary-layer flow of a Powell-Eyring hybrid nanofluid over an inclined plate aligned along the x-axis at $y = 0$, as shown in Figure 6, under the simultaneous effects of a transverse magnetic field and thermal radiation, with no slip between the phases. The magnetic Reynolds number is assumed to be sufficiently small to neglect the induced magnetic field and viscous dissipation.

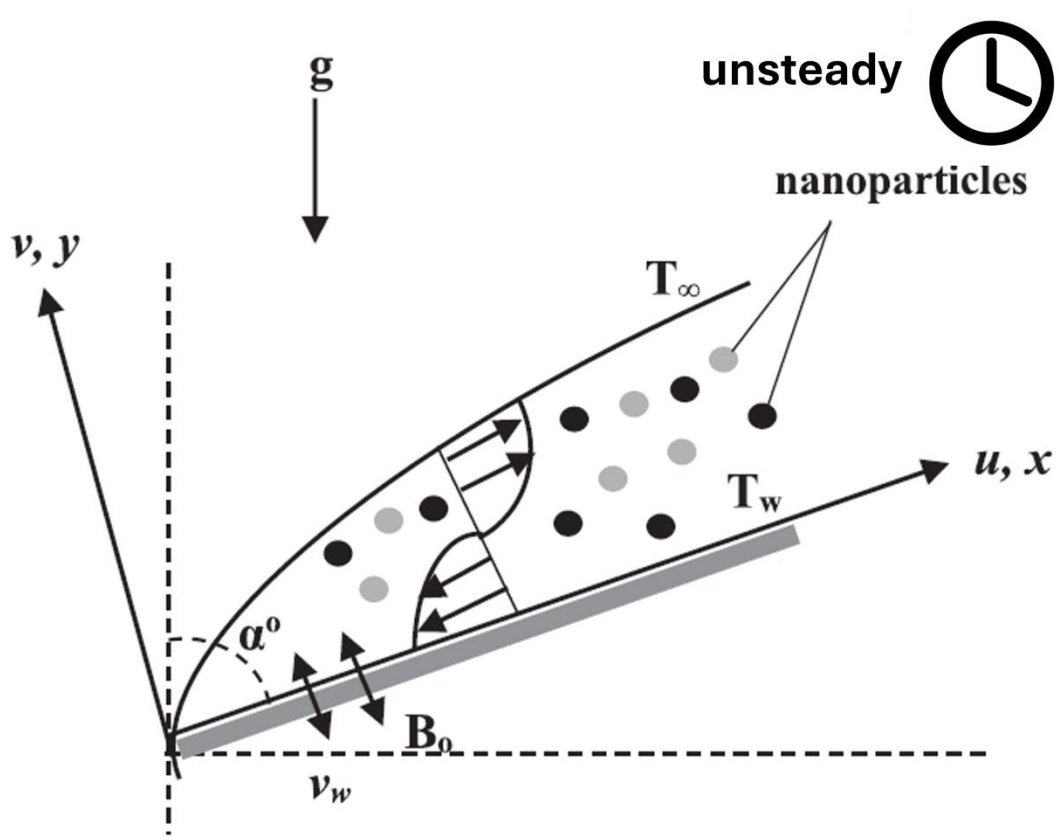

Figure 6: Schematic diagram for problem 1

Figure 6 illustrates the first physical model explored in this research: the unsteady Powell-Eyring hybrid nanofluid flow over an inclined plate under the

influence of a magnetic field and thermal radiation. The schematic depicts the velocity and temperature boundary layers that form due to the interaction of viscous, magnetic, and buoyant forces. The figure also indicates the role of inclination angle α, showing how gravitational components along the plate influence flow stability and heat distribution (Wahid et al., 2023).

To solve this problem, the concerned governing equations can be written in PDE form. The PDEs instantiate the continuum balance laws closed by a rheology and mixture correlations for hybrid effective properties. This governing model stands on the consideration of continuum mechanics and Fourier-Newton transport (combination of conduction inside a fluid with convection at its boundary). By using the boundary layer approximation, the PDE equations with Powell-Eyring model can be reduced to boundary layer equations in the form of PDEs that contains continuity equation (2.1), momentum equation (2.2), and energy equation (2.3), with boundary condition (2.4) and (2.5). The governing equations are as follows (Aziz et al., 2021),

$$\frac{\partial u}{\partial x}+\frac{\partial v}{\partial y}=0 \tag{2.1}$$

$$\frac{\partial u}{\partial t}+u\frac{\partial u}{\partial x}+v\frac{\partial u}{\partial y}=\left(\nu_{hnf}+\frac{1}{\rho_{hnf}\beta\varsigma}\right)\frac{\partial^2 u}{\partial y^2}-\frac{1}{2\beta\varsigma^3\rho_{hnf}}\left(\frac{\partial u}{\partial y}\right)^2\frac{\partial^2 u}{\partial y^2} +g\beta_{hnf}(T-T_\infty)\cos\alpha-\frac{\sigma_{\mathrm{hnf}}B^2}{\rho_{\mathrm{hnf}}}u \tag{2.2}$$

$$\frac{\partial T}{\partial t}+u\frac{\partial T}{\partial x}+v\frac{\partial T}{\partial y}=\frac{k_{\mathrm{hnf}}}{(\rho C_p)_{\mathrm{hnf}}}\left[\frac{\partial^2 T}{\partial y^2}\right]-\frac{1}{(\rho C_p)_{\mathrm{hnf}}}\left[\frac{\partial q_r}{\partial y}\right] \tag{2.3}$$

Where u and v along the x and y directions are velocity components, $\beta=\frac{\beta_0\left(1-\varpi t\right)^{\frac{3}{2}}}{x}$ and $\varsigma=\frac{x\varsigma_0}{\left(1-\varpi t\right)^{\frac{3}{2}}}$ is material constant, ρ_{hnf} is fluid density, C_p is specific heat capacity at constant pressure, $\left(\rho C_p\right)_{hnf}$ is volumetric heat capacity of the hybrid nanofluids (HNFs), g is gravity constant, T is absolute temperature, T_∞ is temperature of undisturbed flowing stream, α is the angle of the stream flow measured from vertical, σ_{hnf} is the electrical conductivity, μ_{hnf} is dynamic viscosity, k_{hnf} is

thermal conductivity, q_r is radiative heat flux. The momentum equation consists of convection with Powell-Eyring diffusion/retardation terms using an effective kinematic viscosity v_{hnf} for hybrid-nanofluid properties. The energy equation consists of convection and conduction with thermal conductivity. The governing equation includes MHD and inclined plate equation into the momentum equation (Aziz et al., 2021).

The MHD term, $-\frac{\sigma_{\text{hnf}} B^2}{\rho_{\text{hnf}}} u$, consist of velocity of the component in the x-direction, u, scale by electrical conductivity of the hybrid nanofluid, σ_{hnf} with applied magnetic field, B over effective density of the nanofluid. This term represents the Lorentz force, and it is negative due to it acting opposite to the fluid motion, hence served as retarding force opposing the velocity u. This form followed the standard Ohmic heating (Escudier & Atkins, 2019). The applied magnetic field, B is defined as $B(t) = B_0 \left(\frac{1}{1-\varpi t} \right)^{\frac{1}{2}}$ whereas $t \to \frac{1}{\omega}$, the magnetic field blows up, approach to unphysical singularities, hence the applied magnetic field would not diverge. However, this model serves as artifact which chosen to simplify the similarity transformation, and it is a classical approximation used by many published works in nanofluid boundary layer studies.

The inclined-plate part is defined by $g\beta_{hnf}(T - T_\infty)\cos\alpha$ where the angle is measured from vertical ($\alpha = 0$ or $\cos\alpha = 1$ for vertical plate, $\alpha = \frac{\pi}{2}$ or $\cos\alpha = 0$ for horizontal plate). It basically describes that the buoyant driving force along the inclined plate scales with the temperature difference between the surface and its surroundings, amplified by the nanofluid's thermal expansion coefficient and gravity, but reduced in proportion to the cosine of the plate's tilt angle from vertical. The positive signs show the flow is increases upslope, and if the plate heated $T > T_\infty$, the term should aid the flow.

The boundary conditions are as follows:

$$u = U_w(x,t) + L\left[\frac{\partial u}{\partial y}\right], \quad v = v_w, \quad -k_{hnf}\left[\frac{\partial T}{\partial y}\right] = h_f(T_w - T) \text{ at } y = 0 \tag{2.4}$$

$$u \to 0, \quad T \to T_\infty \quad \text{as } y \to \infty \tag{2.5}$$

Where $U_w(x,t) = \frac{xc}{1-\varpi t}$ is tangential velocity at wall with $L = L_0(1-\varpi t)^{\frac{1}{2}}$ is the velocity slip factor L_0 scale by $(1-\varpi t)^{\frac{1}{2}}$ for the flow, $v_w = -\left(\frac{\nu_f c}{1-\varpi t}\right)^{\frac{1}{2}} S$ is a normal velocity at wall with S is suction ($v_w < 0$) or injection ($v_w > 0$) parameter. The term $-k_{hnf}\left[\frac{\partial T}{\partial y}\right] = h_f(T_w - T)$ at $y = 0$ is also known as Newtonian heating implemented as convective wall where $T_w(x,t) = T_\infty + \frac{xc}{(1-\varpi t)^2}$ is the temperature at wall, T_∞ is ambient temperature, and $h_f = h_{f0}(1-\varpi t)^{-\frac{1}{2}}$ as the heat transfer coefficient (Aziz et al., 2021).

In order to transform PDE into ODE, the similarity variables η with stream function ψ and dimensionless temperature θ are introduced as (Aziz et al., 2021):

$$\eta(x,y) = \sqrt{\frac{c}{\nu_f(1-\varpi t)}}\, y, \quad \psi(x,y) = \sqrt{\frac{\nu_f c}{1-\varpi t}}\, x f(\eta) \tag{2.6}$$

$$\theta(\eta) = \frac{T - T_\infty}{T_w - T_\infty} \tag{2.7}$$

$$u = \frac{\partial \psi}{\partial y}, \quad v = -\frac{\partial \psi}{\partial x} \tag{2.8}$$

where f and θ is a dimensionless stream function and dimensionless temperature respectively, ν_f is kinematic viscosity.

3.1.1.1 Transformation of Continuity Equation

Finding u from (2.8), we obtain:

$$
\begin{aligned}
u &= \left(\frac{\partial \psi}{\partial \eta}\right)\left(\frac{\partial \eta}{\partial y}\right) \\
&= \frac{\partial}{\partial \eta}\left(\left(\frac{\nu_f c}{1-\varpi t}\right)^{\frac{1}{2}} xf\right)\frac{\partial}{\partial y}\left(\left(\frac{c}{\nu_f (1-\varpi t)}\right)^{\frac{1}{2}} y\right) \\
&= \left(\frac{\nu_f c}{1-\varpi t}\right)^{\frac{1}{2}} xf'\left(\frac{c}{\nu_f (1-\varpi t)}\right)^{\frac{1}{2}} \\
&= \frac{c}{1-\varpi t} xf'
\end{aligned}
\tag{2.9}
$$

where (`) is a differentiation with respect to η.

Finding v from (2.8), we obtain:

$$
\begin{aligned}
v &= -\frac{\partial \psi}{\partial x} \\
&= -\frac{\partial}{\partial x}\left(\left(\frac{\nu_f c}{1-\varpi t}\right)^{\frac{1}{2}} xf\right) \\
&= -\left(\frac{\nu_f c}{1-\varpi t}\right)^{\frac{1}{2}} f
\end{aligned}
\tag{2.10}
$$

To solve continuity equation, differentiating u with respect to x, $\frac{\partial u}{\partial x}$ and differentiating v with respect to y, $\frac{\partial v}{\partial y}$ from (2.9) and (2.10) respectively, we get:

$$
\frac{\partial u}{\partial x} = \frac{\partial}{\partial x}\left(\frac{c}{1-\varpi t} xf'\right) = \frac{c}{1-\varpi t} f' \tag{2.11}
$$

$$\frac{\partial v}{\partial y} = \frac{\partial}{\partial y}\left(-\left(\frac{\nu_f c}{1-\varpi t}\right)^{\frac{1}{2}} f\right)$$

$$= -\left(\frac{\nu_f c}{1-\varpi t}\right)^{\frac{1}{2}} \frac{\partial f}{\partial \eta}\frac{\partial \eta}{\partial y} \tag{2.12}$$

$$= -\left(\frac{\nu_f c}{1-\varpi t}\right)^{\frac{1}{2}} f'\left(\frac{c}{\nu_f (1-\varpi t)}\right)^{\frac{1}{2}}$$

$$= -\frac{c}{1-\varpi t} f'$$

Substitute (2.11) and (2.12) into the continuity equation (2.1):

$$\frac{\partial u}{\partial x} + \frac{\partial v}{\partial y} = \left(\frac{c}{1-\varpi t} f'\right) + \left(-\frac{c}{1-\varpi t} f'\right) = 0 \tag{2.13}$$

Thus, the continuity equation is satisfied.

3.1.1.2 Transformation of momentum equation

Differentiating u with respect to t, $\frac{\partial u}{\partial t}$:

$$\frac{\partial u}{\partial t} = \frac{\partial}{\partial t}\left(\frac{c}{1-\varpi t} x f'(\eta)\right), \text{where } \eta = \left(\frac{c}{\nu_f (1-\varpi t)}\right)^{\frac{1}{2}} y$$

$$\frac{\partial u}{\partial t} = xc\frac{\partial}{\partial t}\left((1-\varpi t)^{-1} f'\right)$$

Let $a = (1-\varpi t)^{-1}$ and $b = f'(\eta)$ where $\eta = \left(\frac{c}{\nu_f (1-\varpi t)}\right)^{\frac{1}{2}} y$

$$\frac{\partial u}{\partial t} = xc\left[ab' + a'b\right]$$

$$= xc\left[(1-\varpi t)^{-1} f''\frac{\partial}{\partial t}\left(\left(\frac{c}{\nu_f (1-\varpi t)}\right)^{\frac{1}{2}} y\right) - (1-\varpi t)^{-2}(-\varpi) f'\right]$$

$$= xc\left[(1-\varpi t)^{-1} f''\left(\frac{c}{\nu_f}\right)^{\frac{1}{2}} y\frac{\partial}{\partial t}\left((1-\varpi t)^{-\frac{1}{2}}\right) - (1-\varpi t)^{-2}(-\varpi) f'\right]$$

$$= xc\left[(1-\varpi t)^{-1} f''\left(\frac{c}{\nu_f}\right)^{\frac{1}{2}} y(-\varpi)\left(-\frac{1}{2}\right)(1-\varpi t)^{-\frac{3}{2}} - (1-\varpi t)^{-2}(-\varpi) f'\right] \quad (2.14)$$

$$= \frac{1}{2}\frac{\varpi c}{(1-\varpi t)(1-\varpi t)^{\frac{3}{2}}} x f''\left(\frac{c}{\nu_f}\right)^{\frac{1}{2}} y + \frac{\varpi c}{(1-\varpi t)^2} x f'$$

$$= \frac{1}{2}\eta\frac{\varpi c}{(1-\varpi t)^2} x f'' + \frac{\varpi c}{(1-\varpi t)^2} x f'$$

Differentiating u with respect to y, $\frac{\partial u}{\partial y}$:

$$
\begin{aligned}
\frac{\partial u}{\partial y} &= \frac{\partial}{\partial y}\left(\frac{c}{1-\varpi t} x f'\right) \\
&= \frac{c}{1-\varpi t} x \frac{\partial}{\partial y}\left(f'\right)\frac{\partial \eta}{\partial \eta} \\
&= \frac{c}{1-\varpi t} x \frac{\partial}{\partial \eta}\left(f'\right)\frac{\partial \eta}{\partial y} \\
&= \frac{c}{1-\varpi t} x f'' \frac{\partial}{\partial y}\left(\sqrt{\frac{c}{\nu_f (1-\varpi t)}} y\right) \\
&= \frac{c}{1-\varpi t}\left(\frac{c}{\nu_f (1-\varpi t)}\right)^{\frac{1}{2}} x f''
\end{aligned}
\tag{2.15}
$$

Then, the $\frac{\partial u}{\partial y}$ is further derived to second order, $\frac{\partial^2 u}{\partial y^2}$:

$$
\begin{aligned}
\frac{\partial^2 u}{\partial y^2} &= \frac{\partial}{\partial y}\left(\frac{c}{1-\varpi t}\left(\frac{c}{\nu_f (1-\varpi t)}\right)^{\frac{1}{2}} x f''\right) \\
&= \frac{c}{1-\varpi t}\left(\frac{c}{\nu_f (1-\varpi t)}\right)^{\frac{1}{2}} x \frac{\partial}{\partial y}\left(f''\right)\left(\frac{\partial \eta}{\partial \eta}\right) \\
&= \frac{c}{1-\varpi t}\left(\frac{c}{\nu_f (1-\varpi t)}\right)^{\frac{1}{2}} x \frac{\partial}{\partial \eta}\left(f''\right)\left(\frac{\partial \eta}{\partial y}\right) \\
&= \frac{c}{1-\varpi t}\left(\frac{c}{\nu_f (1-\varpi t)}\right)^{\frac{1}{2}} x f'''\left(\frac{c}{\nu_f (1-\varpi t)}\right)^{\frac{1}{2}} \\
&= \frac{c}{1-\varpi t}\left(\frac{c}{\nu_f (1-\varpi t)}\right) x f'''
\end{aligned}
\tag{2.16}
$$

The dimensional temperature expression is defined in terms of the similarity variable η, where the wall and ambient temperature difference is expressed through a time-dependent boundary condition as follows:

$$
\begin{aligned}
T &= T_\infty + \theta(\eta)(T_w - T_\infty) \\
&= T_\infty + \theta\left(T_\infty + \frac{cx}{\left(1-\varpi t\right)^2} - T_\infty \right) \\
&= T_\infty + \theta\left(\frac{cx}{\left(1-\varpi t\right)^2} \right)
\end{aligned}
\tag{2.17}
$$

Substitutes (2.9), (2.10), (2.14), (2.15), and (2.16) into the momentum equation (2.2),

$$
\begin{aligned}
&\left(\frac{1}{2}\eta \frac{\varpi c}{\left(1-\varpi t\right)^2} xf'' + \frac{\varpi c}{\left(1-\varpi t\right)^2} xf' \right) + \left(\frac{c}{1-\varpi t} xf' \right)\left(\frac{c}{1-\varpi t} f' \right) \\
&+ \left(-\left(\frac{\nu_f c}{1-\varpi t} \right)^{\frac{1}{2}} f \right)\left(\frac{c}{1-\varpi t}\left(\frac{c}{\nu_f (1-\varpi t)} \right)^{\frac{1}{2}} xf'' \right) \\
&= \left(\nu_{hnf} + \frac{1}{\rho_{hnf}\beta\varsigma} \right)\left(\frac{c}{1-\varpi t}\left(\frac{c}{\nu_f (1-\varpi t)} \right) xf''' \right) \\
&- \frac{1}{2\beta\varsigma^3 \rho_{hnf}}\left(\frac{c}{1-\varpi t}\left(\frac{c}{\nu_f (1-\varpi t)} \right)^{\frac{1}{2}} xf'' \right)^2 \\
&\left(\frac{c}{1-\varpi t}\left(\frac{c}{\nu_f (1-\varpi t)} \right) xf''' \right) - \frac{\sigma_{\text{hnf}}\left(B_0\left(\frac{1}{1-\varpi t} \right)^{\frac{1}{2}} \right)^2}{\rho_{\text{hnf}}}\left(\frac{c}{1-\varpi t} xf' \right) \\
&+ g\beta_{hnf}\left(\left(T_\infty + \theta\left(\frac{cx}{\left(1-\varpi t\right)^2} \right) \right) - T_\infty \right)\cos\alpha
\end{aligned}
\tag{2.18}
$$

Simplify (2.18) by expanding, rearranging, and expressing all terms explicitly in powers of x and derivatives of f.

$$\frac{1}{2}\eta\frac{\varpi c}{\left(1-\varpi t\right)^2}xf''+\frac{\varpi c}{\left(1-\varpi t\right)^2}xf'+\left(\frac{c}{1-\varpi t}\right)^2xf'^2-\left(\frac{c}{1-\varpi t}\right)^2xff''$$
$$=\left(\nu_{hnf}+\frac{1}{\rho_{hnf}\beta\varsigma}\right)\left(\left(\frac{c}{(1-\varpi t)}\right)^2\frac{1}{\nu_f}\right)xf'''$$
$$-\frac{1}{2\beta\varsigma^3\rho_{hnf}}\left(\frac{c}{1-\varpi t}\right)^5\left(\frac{1}{\nu_f}\right)^2x^3f''^2f''' \qquad (2.19)$$
$$-\frac{\sigma_{\mathrm{hnf}}\left(B_0\left(\frac{1}{1-\varpi t}\right)^{\frac{1}{2}}\right)^2}{\rho_{\mathrm{hnf}}}\left(\frac{c}{1-\varpi t}\right)xf'+g\beta_{hnf}\theta\left(\frac{cx}{\left(1-\varpi t\right)^2}\right)\cos\alpha$$

Rearrange all terms in (2.19) to one side of the equation and setting the expression equal to zero.

$$\frac{1}{2\beta\varsigma^3\rho_{hnf}}\left(\frac{c}{1-\varpi t}\right)^5\left(\frac{1}{\nu_f}\right)^2x^3f''^2f'''$$
$$-\left(\nu_{hnf}+\frac{1}{\rho_{hnf}\beta\varsigma}\right)\left(\left(\frac{c}{(1-\varpi t)}\right)^2\frac{1}{\nu_f}\right)xf'''$$
$$-\left(\frac{c}{1-\varpi t}\right)^2xff''+\left(\frac{c}{1-\varpi t}\right)^2xf'^2+\frac{\varpi c}{\left(1-\varpi t\right)^2}xf'+\frac{1}{2}\eta\frac{\varpi c}{\left(1-\varpi t\right)^2}xf'' \qquad (2.20)$$
$$+\frac{\sigma_{\mathrm{hnf}}\left(B_0\left(\frac{1}{1-\varpi t}\right)^{\frac{1}{2}}\right)^2}{\rho_{\mathrm{hnf}}}\left(\frac{c}{1-\varpi t}\right)xf'-g\beta_{hnf}\theta\left(\frac{cx}{\left(1-\varpi t\right)^2}\right)\cos\alpha=0$$

Equation (2.20) is simplified by grouping like terms, particularly combining the third-order derivative terms and reorganizing the expression

$$\left(\frac{1}{2\beta\varsigma^3\rho_{hnf}}\left(\frac{c}{1-\varpi t}\right)^5\left(\frac{1}{\nu_f}\right)^2 x^3 f''^2-\left(\nu_{hnf}+\frac{1}{\rho_{hnf}\beta\varsigma}\right)\left(\frac{c}{1-\varpi t}\right)^2\frac{1}{\nu_f}x\right)f'''$$
$$-\left(\frac{c}{1-\varpi t}\right)^2 xff''+\left(\frac{c}{1-\varpi t}\right)^2 xf'^2+\frac{\varpi c}{(1-\varpi t)^2}xf'+\frac{1}{2}\eta\frac{\varpi c}{(1-\varpi t)^2}xf''$$
$$+\frac{\sigma_{\text{hnf}}\left(B_0\left(\frac{1}{1-\varpi t}\right)^{\frac{1}{2}}\right)^2}{\rho_{\text{hnf}}}\left(\frac{c}{1-\varpi t}\right)xf'-g\beta_{hnf}\theta\left(\frac{cx}{(1-\varpi t)^2}\right)\cos\alpha \qquad (2.21)$$
$$=0$$

Divides all of the term in (2.21) with $\left(\frac{c}{1-\varpi t}\right)^2 x$

$$\left(\frac{1}{2\beta\varsigma^3\rho_{hnf}}\left(\frac{c}{1-\varpi t}\right)^3\left(\frac{1}{\nu_f}\right)^2 x^2 f''^2-\left(\nu_{hnf}+\frac{1}{\rho_{hnf}\beta\varsigma}\right)\frac{1}{\nu_f}\right)f'''$$
$$-ff''+f'^2+\frac{\varpi}{c}f'+\frac{1}{2}\eta\frac{\varpi}{c}f'' \qquad (2.22)$$
$$+\frac{\sigma_{\text{hnf}}\left(B_0\left(\frac{1}{1-\varpi t}\right)^{\frac{1}{2}}\right)^2}{\rho_{\text{hnf}}}\left(\frac{1-\varpi t}{c}\right)f'-g\beta_{hnf}\theta\left(\frac{1}{c}\right)\cos\alpha=0$$

Substitutes β and ς equations into (2.22)

$$\left(\begin{array}{l}\dfrac{1}{2\left(\dfrac{\beta_0\left(1-\varpi t\right)^{\frac{3}{2}}}{x}\right)\left(\dfrac{x\varsigma_0}{\left(1-\varpi t\right)^{\frac{3}{2}}}\right)^3\rho_{hnf}}\left(\dfrac{c}{1-\varpi t}\right)^3\left(\dfrac{1}{\nu_f}\right)^2 x^2 f''^2 \\ -\left(\nu_{hnf}+\dfrac{1}{\rho_{hnf}\left(\dfrac{\beta_0\left(1-\varpi t\right)^{\frac{3}{2}}}{x}\right)\left(\dfrac{x\varsigma_0}{\left(1-\varpi t\right)^{\frac{3}{2}}}\right)}\right)\dfrac{1}{\nu_f}\end{array}\right) f'''$$

$$-ff''+f'^2+\frac{\varpi}{c}f'+\frac{1}{2}\eta\frac{\varpi}{c}f'' \qquad (2.23)$$

$$+\frac{\sigma_{\text{hnf}}\left(B_0\left(\dfrac{1}{1-\varpi t}\right)^{\frac{1}{2}}\right)^2}{\rho_{\text{hnf}}}\left(\frac{1-\varpi t}{c}\right)f'-g\beta_{hnf}\theta\left(\frac{1}{c}\right)\cos\alpha=0$$

Simplifies (2.23),

$$\left(\frac{c^3}{2\beta_0\varsigma_0^3\rho_{hnf}}\left(\frac{1}{\nu_f}\right)^2 f''^2-\left(\nu_{hnf}+\frac{1}{\rho_{hnf}\beta_0\varsigma_0}\right)\frac{1}{\nu_f}\right)f'''$$

$$-ff''+f'^2+\frac{\varpi}{c}f'+\frac{1}{2}\eta\frac{\varpi}{c}f'' \qquad (2.24)$$

$$+\frac{\sigma_{\text{hnf}}\left(B_0\left(\dfrac{1}{1-\varpi t}\right)^{\frac{1}{2}}\right)^2}{\rho_{\text{hnf}}}\frac{\left(1-\varpi t\right)}{c}f'-g\beta_{hnf}\theta\left(\frac{1}{c}\right)\cos\alpha=0$$

Let $\nu_f=\dfrac{\mu_f}{\rho_f}$ and $\nu_{hnf}=\dfrac{\mu_{hnf}}{\rho_{hnf}}$

$$\left(\frac{c^3}{2\beta_0\varsigma_0^3\rho_{hnf}}\left(\frac{1}{\nu_f}\right)\left(\frac{\rho_f}{\mu_f}\right)f''^2-\left(\left(\frac{\mu_{hnf}}{\rho_{hnf}}\right)+\frac{1}{\rho_{hnf}\beta_0\varsigma_0}\right)\frac{\rho_f}{\mu_f}\right)f'''$$
$$-ff''+f'^2+\frac{\varpi}{c}f'+\frac{1}{2}\eta\frac{\varpi}{c}f'' \qquad (2.25)$$
$$+\frac{\sigma_{\text{hnf}}\left(B_0\left(\frac{1}{1-\varpi t}\right)^{\frac{1}{2}}\right)^2}{\rho_{\text{hnf}}}\frac{(1-\varpi t)}{c}f'-g\beta_{hnf}\theta\left(\frac{1}{c}\right)\cos\alpha=0$$

Reformulate (2.25) by factoring and rearranging terms to explicitly identify physical parameters, simplifying the equation into a dimensionless form suitable for physical interpretation.

$$\left(\frac{c^3}{2\varsigma_0^2\nu_f}\left(\frac{1}{\mu_f\beta_0\varsigma_0}\right)\frac{\rho_f}{\rho_{hnf}}f''^2-\left(\frac{\mu_{hnf}}{\mu_f}+\frac{1}{\mu_f\beta_0\varsigma_0}\right)\frac{\rho_f}{\rho_{hnf}}\right)f'''$$
$$-ff''+f'^2+\frac{\varpi}{c}f'+\frac{1}{2}\eta\frac{\varpi}{c}f'' \qquad (2.26)$$
$$+\frac{\sigma_{\text{hnf}}B_0^2}{\rho_{\text{hnf}}}f'-\left(\frac{g\beta_f}{c}\right)\left(\frac{\beta_{hnf}}{\beta_f}\right)\theta\cos\alpha=0$$

Divide (2.26) with $\frac{\rho_f}{\rho_{hnf}}$

$$\left(\frac{c^3}{2\varsigma_0^2\nu_f}\left(\frac{1}{\mu_f\beta_0\varsigma_0}\right)f''^2-\left(\frac{\mu_{hnf}}{\mu_f}+\frac{1}{\mu_f\beta_0\varsigma_0}\right)\right)f'''$$
$$-\frac{\rho_{hnf}}{\rho_f}ff''+\frac{\rho_{hnf}}{\rho_f}f'^2+\frac{\varpi}{c}\frac{\rho_{hnf}}{\rho_f}f'+\frac{1}{2}\eta\frac{\varpi}{c}\frac{\rho_{hnf}}{\rho_f}f'' \qquad (2.27)$$
$$+\frac{\sigma_{\text{hnf}}B_0^2}{\rho_f}\left(\frac{\sigma_{\text{f}}}{\sigma_{\text{f}}}\right)f'-\left(\frac{g\beta_f}{c}\right)\left(\frac{\beta_{hnf}}{\beta_f}\right)\frac{\rho_{hnf}}{\rho_f}\theta\cos\alpha=0$$

The ODE for the momentum equation:

$$\left(\omega\left(\Delta f''^2-1\right)-\phi_\mu\right)f'''+\phi_\rho\left(f'^2-ff''+A\left(f'+\frac{\eta}{2}f''\right)-\phi_\beta\lambda\theta\cos\alpha\right)+\phi_\sigma Mf'=0 \qquad (2.28)$$

where $\Delta = \frac{c^3}{2\varsigma_0^2 \nu_f}$ and $\omega = \frac{1}{\mu_f \beta_0 \varsigma_0}$ are material parameters, $A = \frac{\varpi}{c}$ is unsteadiness parameter, $M = \frac{\sigma_f B_0^2}{\rho_f c}$ is magnetic field parameter, $\lambda = \frac{g\beta_f}{c} = \frac{Gr}{\mathrm{Re}_x^2}$ is buoyancy parameter, and $\phi_\mu = \frac{\mu_{hnf}}{\mu_f}, \phi_\rho = \frac{\rho_{hnf}}{\rho_f}, \phi_\beta = \frac{\beta_{hnf}}{\beta_f}, \phi_\sigma = \frac{\sigma_{hnf}}{\sigma_f}$ is ratio between hybrid nanofluid and base fluid on viscosity, density, thermal expansion coefficient, and electrical conductivity respectively.

3.1.1.3 Transformation of energy equation

The temperature, T is being differentiate with respect to x, $\frac{\partial T}{\partial x}$:

$$\begin{aligned}
&\frac{\partial T}{\partial x} = \frac{\partial}{\partial x}\left[T_\infty + \theta(\eta)(T_w - T_\infty)\right] \\
&= \frac{\partial}{\partial x}\left[T_\infty + \theta \frac{xc}{\left(1-\varpi t\right)^2}\right] \\
&= \frac{c}{\left(1-\varpi t\right)^2}\theta
\end{aligned} \tag{2.29}$$

Then temperature, T is being differentiate with respect to y, $\frac{\partial T}{\partial y}$:

$$\begin{aligned}
&\frac{\partial T}{\partial y} = \frac{\partial}{\partial y}\left[T_\infty + \theta(\eta)(T_w - T_\infty)\right] \\
&= (T_w - T_\infty)\frac{d\theta}{d\eta}\frac{d\eta}{dy} \\
&= (T_w - T_\infty)\left(\frac{c}{\nu_f(1-\varpi t)}\right)^{\frac{1}{2}}\theta' \\
&= \left(\frac{xc}{\left(1-\varpi t\right)^2}\right)\left(\frac{c}{\nu_f(1-\varpi t)}\right)^{\frac{1}{2}}\theta'
\end{aligned} \tag{2.30}$$

The temperature, T is then being further differentiate to 2nd order with respect to y, $\frac{\partial^2 T}{\partial y^2}$:

$$\begin{aligned}
\frac{\partial^2 T}{\partial y^2} &= \frac{\partial}{\partial y}\left[(T_w - T_\infty)\left(\frac{c}{\nu_f(1-\varpi t)}\right)^{\frac{1}{2}}\theta'\right] \\
&= (T_w - T_\infty)\left(\frac{c}{\nu_f(1-\varpi t)}\right)^{\frac{1}{2}}\frac{\partial}{\partial \eta}[\theta']\frac{\partial \eta}{\partial y} \\
&= (T_w - T_\infty)\left(\frac{c}{\nu_f(1-\varpi t)}\right)^{\frac{1}{2}}\theta''\left(\frac{c}{\nu_f(1-\varpi t)}\right)^{\frac{1}{2}} \\
&= \frac{xc}{(1-\varpi t)^2}\left(\frac{c}{\nu_f(1-\varpi t)}\right)\theta''
\end{aligned} \tag{2.31}$$

The temperature then being differentiate with respect to time:

$$
\begin{aligned}
&\frac{\partial T}{\partial t} = \frac{\partial}{\partial t}\left[T_\infty + \theta(T_w - T_\infty)\right] \\
&= 0 + \frac{\partial}{\partial t}\left[\theta(T_w - T_\infty)\right] \\
&= \frac{\partial}{\partial t}\left[(T_w - T_\infty)\right]\theta + \frac{\partial}{\partial t}\left[\theta\right](T_w - T_\infty) \\
&= \frac{\partial}{\partial t}\left(\left(T_\infty + \frac{xc}{(1-\varpi t)^2}\right) - T_\infty\right)\theta + \frac{\partial}{\partial \eta}\left[\theta\right]\left(\frac{\partial \eta}{\partial t}\right)\left(\left(T_\infty + \frac{xc}{(1-\varpi t)^2}\right) - T_\infty\right) \\
&= \frac{\partial}{\partial t}\left(\frac{xc}{(1-\varpi t)^2}\right)\theta(\eta) + \frac{\partial}{\partial \eta}\left[\theta\right]\left(\frac{\partial \eta}{\partial t}\right)\left(\frac{xc}{(1-\varpi t)^2}\right) \\
&= \frac{\partial}{\partial t}\left(\frac{xc}{(1-\varpi t)^2}\right)\theta + \frac{\partial}{\partial t}\left(\left(\frac{c}{\nu_f(1-\varpi t)}\right)^{\frac{1}{2}} y\right)\left(\frac{xc}{(1-\varpi t)^2}\right)\theta' \\
&= \frac{\partial}{\partial t}(1-\varpi t)^{-2}\, xc\theta + \frac{\partial}{\partial t}\left((1-\varpi t)^{-\frac{1}{2}}\right)\left(\frac{c}{\nu_f}\right)^{\frac{1}{2}} y\left(\frac{xc}{(1-\varpi t)^2}\right)\theta' \\
&= (-2)(-\varpi)(1-\varpi t)^{-3}\, xc\theta + \frac{\varpi}{2}(1-\varpi t)^{-\frac{3}{2}}\left(\frac{c}{\nu_f}\right)^{\frac{1}{2}} y\left(\frac{xc}{(1-\varpi t)^2}\right)\theta' \\
&= \frac{2\varpi xc}{(1-\varpi t)^3}\theta + \frac{\varpi}{2(1-\varpi t)}\left(\frac{xc}{(1-\varpi t)^2}\right)\left(\frac{c}{\nu_f(1-\varpi t)}\right)^{\frac{1}{2}} y\theta' \\
&= \frac{2\varpi xc}{(1-\varpi t)^3}\theta + \frac{\varpi}{2(1-\varpi t)}\left(\frac{xc}{(1-\varpi t)^2}\right)\eta\theta'
\end{aligned}
\tag{2.32}
$$

The radiative heat flux q_r based on the Rosseland approximation is expressed as follows, incorporating the temperature field expansion and similarity transformations:

$$
\begin{aligned}
q_r &= -\frac{4\sigma^*}{3k^*}\frac{\partial T^4}{\partial y} \\
&= -\frac{4\sigma^*}{3k^*}\frac{\partial}{\partial y}\left[4T_\infty^3 T - 3T_\infty^4\right] \\
&= -\frac{4\sigma^*}{3k^*}\frac{\partial}{\partial y}\left[4T_\infty^3 T\right] \\
&= -\frac{16\sigma^* T_\infty^3}{3k^*}\frac{\partial T}{\partial y} \\
&= -\frac{16\sigma^* T_\infty^3}{3k^*}\left((T_w - T_\infty)\left(\frac{c}{\nu_f(1-\varpi t)}\right)^{\frac{1}{2}}\theta'\right) \\
&= -\frac{16\sigma^* T_\infty^3}{3k^*}\left(\frac{xc}{(1-\varpi t)^2}\left(\frac{c}{\nu_f(1-\varpi t)}\right)^{\frac{1}{2}}\theta'\right)
\end{aligned}
\tag{2.33}
$$

The radiative heat flux q_r is differentiated with respect to y, $\frac{\partial q_r}{\partial y}$:

$$
\begin{aligned}
\frac{\partial q_r}{\partial y} &= \frac{\partial}{\partial y}\left(-\frac{16\sigma^* T_\infty^3}{3k^*}\left(\frac{xc}{(1-\varpi t)^2}\left(\frac{c}{\nu_f(1-\varpi t)}\right)^{\frac{1}{2}}\theta'\right)\right) \\
&= -\frac{16\sigma^* T_\infty^3}{3k^*}\left(\frac{xc}{(1-\varpi t)^2}\left(\frac{c}{\nu_f(1-\varpi t)}\right)^{\frac{1}{2}}\right)\frac{\partial}{\partial y}(\theta')\left(\frac{\partial \eta}{\partial \eta}\right) \\
&= -\frac{16\sigma^* T_\infty^3}{3k^*}\left(\frac{xc}{(1-\varpi t)^2}\left(\frac{c}{\nu_f(1-\varpi t)}\right)^{\frac{1}{2}}\right)\frac{\partial}{\partial \eta}(\theta')\left(\frac{\partial \eta}{\partial y}\right) \\
&= -\frac{16\sigma^* T_\infty^3}{3k^*}\left(\frac{xc}{(1-\varpi t)^2}\left(\frac{c}{\nu_f(1-\varpi t)}\right)^{\frac{1}{2}}\right)\theta''\left(\frac{c}{\nu_f(1-\varpi t)}\right)^{\frac{1}{2}} \\
&= -\frac{16\sigma^* T_\infty^3}{3k^*}\left(\frac{xc}{(1-\varpi t)^2}\left(\frac{c}{\nu_f(1-\varpi t)}\right)\right)\theta''
\end{aligned}
\tag{2.34}
$$

Substitutes (2.9), (2.10), (2.29), (2.30), (2.31), and (2.34) into the energy equation (2.3):

$$\left(\frac{2\varpi xc}{(1-\varpi t)^3}\theta+\frac{\varpi}{2(1-\varpi t)}\left(\frac{xc}{(1-\varpi t)^2}\right)\eta\theta'\right)$$
$$+\left(\frac{c}{1-\varpi t}xf'\right)\left(\frac{c}{(1-\omega t)^2}\theta\right)$$
$$+\left(-\left(\frac{\nu_f c}{1-\varpi t}\right)^{\frac{1}{2}}f\right)\left(\left(\frac{xc}{(1-\varpi t)^2}\right)\left(\frac{c}{\nu_f(1-\varpi t)}\right)^{\frac{1}{2}}\theta'\right) \qquad (2.35)$$
$$=\frac{k_{\text{hnf}}}{(\rho C_p)_{\text{hnf}}}\left[\left(\frac{xc}{(1-\varpi t)^2}\right)\left(\frac{c}{\nu_f(1-\varpi t)}\right)\theta''\right]$$
$$-\frac{1}{(\rho C_p)_{\text{hnf}}}\left[-\frac{16\sigma^* T_\infty^3}{3k^*}\left(\left(\frac{xc}{(1-\varpi t)^2}\right)\left(\frac{c}{\nu_f(1-\varpi t)}\right)\theta''\right)\right]$$

Expend the equation (2.35)

$$\frac{2\varpi xc}{(1-\varpi t)^3}\theta+\frac{\varpi}{2(1-\varpi t)}\left(\frac{xc}{(1-\varpi t)^2}\right)\eta\theta'$$
$$+\left(\frac{c}{1-\varpi t}\right)\left(\frac{c}{(1-\varpi t)^2}\right)xf'\theta$$
$$-\left(\frac{c}{(1-\varpi t)^2}\right)\left(\frac{\nu_f c}{1-\varpi t}\right)^{\frac{1}{2}}\left(\frac{c}{\nu_f(1-\varpi t)}\right)^{\frac{1}{2}}xf\theta' \qquad (2.36)$$
$$=\left(\frac{xc}{(1-\varpi t)^2}\right)\frac{k_{\text{hnf}}}{(\rho C_p)_{\text{hnf}}}\left(\frac{c}{\nu_f(1-\varpi t)}\right)\theta''$$
$$+\left(\frac{xc}{(1-\varpi t)^2}\right)\frac{1}{(\rho C_p)_{\text{hnf}}}\left(\frac{c}{\nu_f(1-\varpi t)}\right)\frac{16\sigma^* T_\infty^3}{3k^*}\theta''$$

Rearrange (2.36)

$$\frac{xc}{(1-\varpi t)^2}\frac{k_{\text{hnf}}}{(\rho C_p)_{\text{hnf}}}\left(\frac{c}{\nu_f(1-\varpi t)}\right)\theta''$$
$$+\frac{xc}{(1-\varpi t)^2}\frac{1}{(\rho C_p)_{\text{hnf}}}\left(\frac{c}{\nu_f(1-\varpi t)}\right)\frac{16\sigma^* T_\infty^3}{3k^*}\theta''$$
$$+\frac{c}{(1-\varpi t)^2}\left(\frac{\nu_f c}{1-\varpi t}\right)^{\frac{1}{2}}\left(\frac{c}{\nu_f(1-\varpi t)}\right)^{\frac{1}{2}} xf\,\theta'$$
$$-\left(\frac{c}{1-\varpi t}\right)\left(\frac{c}{(1-\varpi t)^2}\right)xf'\theta \qquad (2.37)$$
$$-\frac{2\varpi xc}{(1-\varpi t)^3}\theta$$
$$-\frac{\varpi}{2(1-\varpi t)}\left(\frac{xc}{(1-\varpi t)^2}\right)\eta\theta' = 0$$

Simplify (2.37)

$$\frac{xc}{(1-\varpi t)^2}\frac{k_{\text{hnf}}}{(\rho C_p)_{\text{hnf}}}\left(\frac{c}{\nu_f(1-\varpi t)}\right)\theta''$$
$$+\frac{xc}{(1-\varpi t)^2}\frac{1}{(\rho C_p)_{\text{hnf}}}\left(\frac{c}{\nu_f(1-\varpi t)}\right)\frac{16\sigma^* T_\infty^3}{3k^*}\theta''$$
$$+\frac{c}{(1-\varpi t)^2}\left(\frac{c}{1-\varpi t}\right)xf\,\theta'$$
$$-\left(\frac{c}{(1-\varpi t)^2}\right)\left(\frac{c}{1-\varpi t}\right)xf'\theta \qquad (2.38)$$
$$-\frac{2\varpi xc}{(1-\varpi t)^3}\theta$$
$$-\frac{\varpi}{2(1-\varpi t)}\left(\frac{xc}{(1-\varpi t)^2}\right)\eta\theta' = 0$$

Divide (2.38) with $\frac{c^2}{(1-\varpi t)^3}x$

$$\frac{1-\varpi t}{c}\frac{k_{\text{hnf}}}{(\rho C_p)_{\text{hnf}}}\left(\frac{c}{\nu_f(1-\varpi t)}\right)\theta'' + \frac{1}{(\rho C_p)_{\text{hnf}}}\left(\frac{1}{\nu_f}\right)\frac{16\sigma^* T_\infty^3}{3k^*}\theta'' + f\theta' - f'\theta - \frac{2\varpi}{c}\theta - \frac{\varpi}{2(1-\varpi t)}\left(\frac{1-\varpi t}{c}\right)\eta\theta' = 0 \quad (2.39)$$

Simplify (2.39)

$$\frac{k_{\text{hnf}}}{(\rho C_p)_{\text{hnf}}}\left(\frac{1}{\nu_f}\right)\theta'' + \frac{1}{(\rho C_p)_{\text{hnf}}}\left(\frac{1}{\nu_f}\right)\frac{16\sigma^* T_\infty^3}{3k^*}\theta'' + f\theta' - f'\theta - 2\left(\frac{\varpi}{c}\right)\theta - \frac{1}{2}\left(\frac{\varpi}{c}\right)\eta\theta' = 0 \quad (2.40)$$

Reformulate (2.40) by factoring and rearranging terms to explicitly identify physical parameters, simplifying the equation into a dimensionless form suitable for physical interpretation.

$$\frac{k_{\text{f}}}{\nu_f(\rho C_p)_{\text{f}}}\left(\frac{(\rho C_p)_{\text{f}}}{(\rho C_p)_{\text{hnf}}}\right)\left(\frac{k_{\text{hnf}}}{k_{\text{f}}}\right)\theta'' + \frac{k_{\text{f}}}{\nu_f(\rho C_p)_{\text{f}}}\left(\frac{(\rho C_p)_{\text{f}}}{(\rho C_p)_{\text{hnf}}}\right)\left(\frac{4}{3}\right)\frac{4\sigma^* T_\infty^3}{k_{\text{f}}k^*}\theta'' + f\theta' - f'\theta - 2\left(\frac{\varpi}{c}\right)\theta - \frac{\eta}{2}\left(\frac{\varpi}{c}\right)\theta' = 0 \quad (2.41)$$

The 2nd order ODE for the energy equation:

$$\left(\frac{(\rho C_p)_{\text{f}}}{(\rho C_p)_{\text{hnf}}}\right)\left[\frac{1}{\text{Pr}}\left(\left(\frac{k_{\text{hnf}}}{k_{\text{f}}}\right)+\left(\frac{4}{3}\right)Rd\right)\theta''\right] - \theta f' + \theta' f - A\left(2\theta + \frac{\eta}{2}\theta'\right) = 0 \quad (2.42)$$

where $A = \frac{\varpi}{c}$ is unsteadiness parameter, $\text{Pr} = \frac{\nu_f(\rho C_p)_{\text{f}}}{k_{\text{f}}}$ is Prandtl number, and $Rd = \frac{4\sigma^* T_\infty^3}{k_{\text{f}}k^*}$ is radiation parameter.

3.1.1.4 Transformation of boundary condition equation

Boundary conditions at $y = 0$, equation (2.6) implies

$$\eta(x,0) = \sqrt{\frac{c}{\nu_f(1-\varpi t)}}(0)$$
$$\eta(0) = 0 \tag{2.43}$$

Taking the v_w into consideration, therefore the boundary conditions for v is,

$$v = v_w \tag{2.44}$$

$$-\left(\frac{\nu_f c}{1-\varpi t}\right)^{\frac{1}{2}} f(0) = -\left(\frac{\nu_f c}{1-\varpi t}\right)^{\frac{1}{2}} S \tag{2.45}$$

$$f(0) = S \tag{2.46}$$

Substitute U_w and L, (2.9), and (2.15) into the boundary conditions for u (2.4) :

$$\frac{c}{1-\varpi t} xf'(0) = \frac{cx}{1-\varpi t} + L\left(\frac{c}{1-\varpi t}\left(\frac{c}{\nu_f(1-\varpi t)}\right)^{\frac{1}{2}} xf''(0)\right) \tag{2.47}$$

Divide (2.47) by $\frac{cx}{1-\varpi t}$

$$\begin{aligned} f'(0) &= 1 + L\left(\frac{c}{\nu_f(1-\varpi t)}\right)^{\frac{1}{2}} f''(0) \\ &= 1 + \left(L_0(1-\varpi t)^{\frac{1}{2}}\right)\left(\frac{c}{\nu_f(1-\varpi t)}\right)^{\frac{1}{2}} f''(0) \\ &= 1 + L_0\left(\frac{c}{\nu_f}\right)^{\frac{1}{2}} f''(0) \\ &= 1 + \Omega f''(0) \end{aligned} \tag{2.48}$$

where $\Omega = L_0\left(\frac{c}{\nu_f}\right)^{\frac{1}{2}}$ is transitional scaling constant of the mass transfer rate.

By inserting (2.17) and (2.30) into (2.4), the boundary conditions for θ is,

$$-k_{hnf}\left[\left(\frac{xc}{\left(1-\varpi t\right)^2}\right)\left(\frac{c}{\nu_f(1-\varpi t)}\right)^{\frac{1}{2}}\theta'\right]$$
$$=h_f\left(\left(T_\infty+\frac{xc}{\left(1-\varpi t\right)^2}\right)-\left(T_\infty+\theta\left(\frac{cx}{\left(1-\varpi t\right)^2}\right)\right)\right) \tag{2.49}$$

Simplify (2.49),

$$\theta'(0)=-\frac{h_f}{k_{hnf}}\left(\frac{\nu_f(1-\varpi t)}{c}\right)^{\frac{1}{2}}\left(1+\theta(0)\right)$$
$$=-\frac{h_f}{k_{hnf}}\left(\frac{\nu_f}{c}\right)^{\frac{1}{2}}\left(1-\theta(0)\right) \tag{2.50}$$
$$=-Bi\left(1-\theta(0)\right)$$

where $Bi=\frac{h_f}{k_{hnf}}\left(\frac{\nu_f}{c}\right)^{\frac{1}{2}}$ is the Biot number.

The second boundary condition (2.5) is applied to the similarity variable (2.6)-(2.8) as follows:

Boundary conditions as $y\to\infty$, equation (2.6) implies $\eta\to\infty$.

Boundary conditions as $u\to 0$, implies,

$$\frac{c}{1-\varpi t}xf'(\infty)\to 0 \tag{2.51}$$

$$f'(\infty)\to 0 \tag{2.52}$$

Boundary conditions as $T\to T_\infty$, equation (2.6) implies,

$$T_\infty+\theta(\infty)(T_w-T_\infty)\to T_\infty \tag{2.53}$$

$$\theta(\infty)(T_w-T_\infty)\to 0 \tag{2.54}$$

$$\theta(\infty)\to 0 \tag{2.55}$$

3.1.2 Problem 2: The impact of MHD & joule heating on steady Powell-Eyring flow over a horizontal flat surface with thermal radiation.

For this problem, a two-dimensional (2D), incompressible, laminar, homogeneous mixture, thermophysical properties as per Maxwell-Garnett/Brinkman, steady boundary-layer flow of a Powell-Eyring hybrid nanofluid over an horizontal plate on x-axis at $y = 0$ as shown in Figure 7, under the simultaneous effects of a transverse magnetic field, thermal radiation and Joule heating with no slip between the phases. The magnetic Reynolds number is assumed small enough to neglect the induced magnetic field and viscous dissipation.

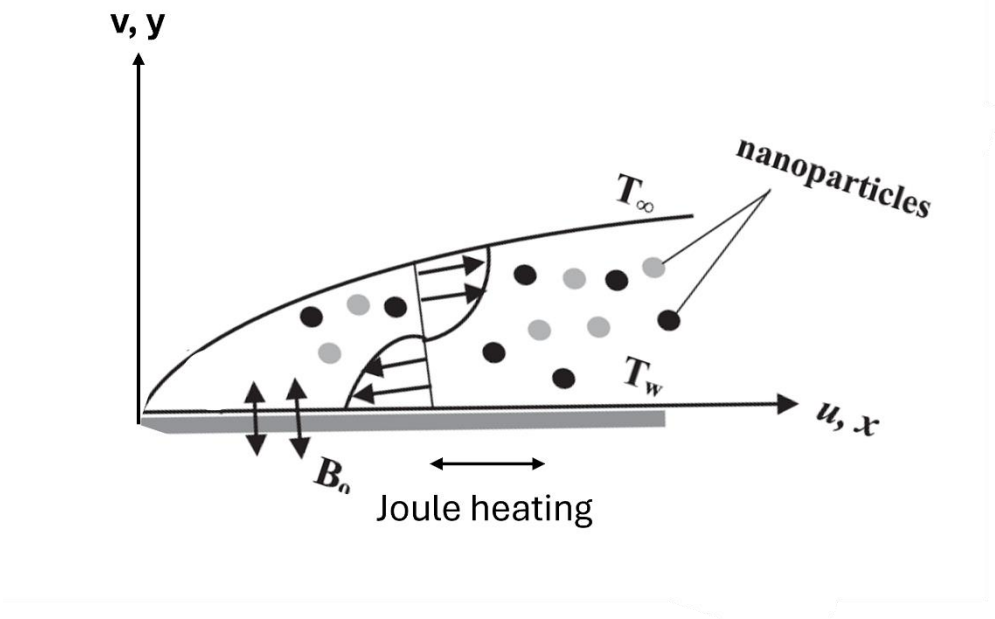

Figure 7: Schematic diagram for problem 2

Figure 7 illustrates the configuration of Problem 2, which investigates the steady Powell-Eyring hybrid nanofluid flow over a horizontal flat surface under the combined effects of magnetohydrodynamics (MHD), Joule heating, and thermal radiation. In this setup, the time-independent, steady-state conditions to reflect a continuous heating environment typical of flat solar collector channels. The schematic shows how the Lorentz force interacts with Ohmic (Joule) dissipation, where electrical energy converts into thermal energy as a conducting fluid moves through a magnetic field. The diagram

thus visualizes how these physical interactions shape the momentum and energy boundary layers, supporting the development of reduced steady-state equations.

By using the boundary layer approximation, the PDE equations with Powell-Eyring model for problem 2 can be reduced to boundary layer equations in the form of PDEs that contains continuity equation (2.56), momentum equation (2.57), and energy equation (2.58), with boundary condition (2.59) and (2.60). The governing equations are as follows (Aminuddin et al., 2024),

$$\frac{\partial u}{\partial x}+\frac{\partial v}{\partial y}=0 \tag{2.56}$$

$$u\frac{\partial u}{\partial x}+v\frac{\partial u}{\partial y}=\left(\nu_{hnf}+\frac{1}{\rho_{hnf}\beta\varsigma}\right)\frac{\partial^2 u}{\partial y^2}-\frac{1}{2\beta\varsigma^3\rho_{hnf}}\left(\frac{\partial u}{\partial y}\right)^2\frac{\partial^2 u}{\partial y^2} -\frac{\sigma_{\mathrm{hnf}}B^2}{\rho_{\mathrm{hnf}}}u \tag{2.57}$$

$$u\frac{\partial T}{\partial x}+v\frac{\partial T}{\partial y}=\frac{k_{\mathrm{hnf}}}{(\rho C_p)_{\mathrm{hnf}}}\left[\frac{\partial^2 T}{\partial y^2}\right]-\frac{1}{(\rho C_p)_{\mathrm{hnf}}}\left[\frac{\partial q_r}{\partial y}\right]+\frac{\sigma_{hnf}B_0^2}{\left(\rho C_p\right)_{hnf}}u \tag{2.58}$$

Subject to boundary conditions,

$$u=U_w(x),\quad v=0,\ T=T_\infty \text{ at } y=0 \tag{2.59}$$

$$u=0,\ T=T_\infty \text{ at } y\to\infty \tag{2.60}$$

The governing equation and boundary layer are modified suitable for the concerned flow. The Joule heating term is defined as $\frac{\sigma_{hnf}B_0^2}{\left(\rho C_p\right)_{hnf}}u$ (Naseem et al., 2023). It comes from the Ohmic dissipation of current in an electrically conducting fluid under a magnetic field. The Joule heating term says that the fluid gets hotter when a conducting fluid moves through a magnetic field with the heat generated growing as the square of the field strength, B_0^2.

The Joule heating is the conversion of electrical energy into thermal energy due to resistance in conducting fluid. It works well with MHD because the rise in fluid

temperature by the Joule heating helps balance out the loss of momentum caused by the Lorentz force.

To obtain the ordinary differential equation (ODEs) from the model, similarity variables need to be implemented, which are given for steady flow as (Aminuddin et al., 2024),

$$
\begin{aligned}
&u = \frac{\partial \psi}{\partial y}, \quad v = -\frac{\partial \psi}{\partial x}, \\
&\eta(x,y) = \sqrt{\frac{c}{\nu_f}}\, y, \;\; \psi(x,y) = \sqrt{\nu_f c}\, x f(\eta), \\
&\theta(\eta) = \frac{T - T_w}{T_w - T_\infty}
\end{aligned}
\tag{2.61}
$$

This similarity equations are necessary to converts a messy, coupled, time-dependent 2-D Newtonian boundary layer system into a boundary-value problem in η .

3.1.3 Problem 3: The influence of MHD and Joule heating on steady Powell-Eyring flow over a vertical plate in porous medium with thermal radiation.

For this problem, a two-dimensional (2D), incompressible, laminar, homogeneous mixture, thermophysical properties as per Maxwell-Garnett/Brinkman, steady boundary-layer flow of a Powell-Eyring hybrid nanofluid over an vertical plate on x-axis at $y = 0$ in porous medium as shown in Figure 8, under the simultaneous effects of a transverse magnetic field, thermal radiation and Joule heating with no slip between the phases. The magnetic Reynolds number is assumed small enough to neglect the induced magnetic field and viscous dissipation.

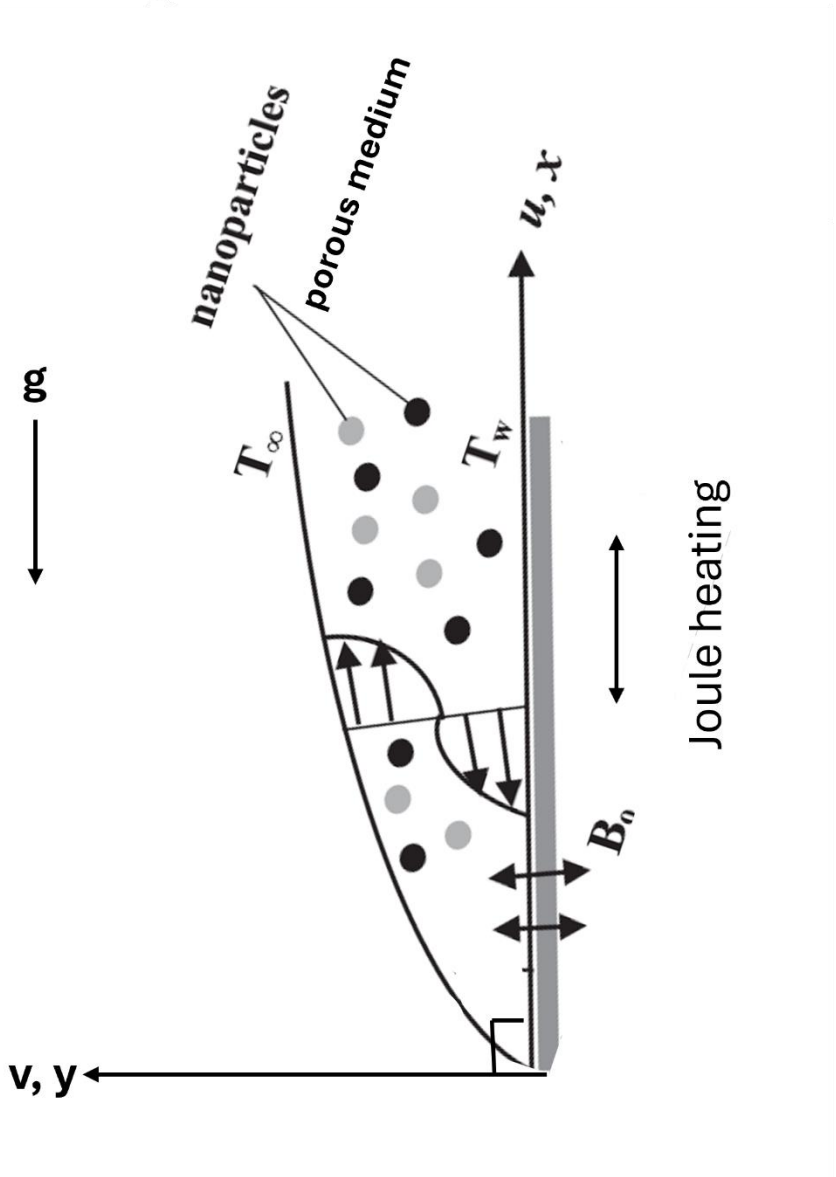

Figure 8: Schematic diagram for problem 3

Figure 8 presents the schematic configuration for Problem 3, which examines the steady Powell-Eyring hybrid nanofluid flow over a vertical plate embedded in a porous medium, influenced by both magnetohydrodynamics (MHD) and Joule heating under thermal radiation conditions. In this setup, the porous layer imposes a resistive drag on the flow that is proportional to the fluid viscosity and inversely proportional to the Darcy permeability, reducing the velocity and thereby thickening the thermal boundary layer. The interaction between magnetic field strength (B_0), permeability, and Joule dissipation governs the rate of heat transfer through the porous medium. As shown in the diagram, the inclusion of Newtonian heating at the wall enhances surface-to-fluid heat exchange, simulating practical energy systems like porous solar receivers or

thermal insulation structures. This configuration extends the preceding problems by coupling MHD-porous resistance effects, providing a more realistic model for complex industrial heat-transfer environments.

By using the boundary layer approximation, the PDE equations with Powell-Eyring model for problem 2 can be reduced to boundary layer equations in the form of PDEs that contains continuity equation (2.62), momentum equation (2.63), and energy equation (2.64), with boundary condition (2.65) and (2.66). The governing equations are as follows (Hahim et al., 2023),

$$\frac{\partial u}{\partial x}+\frac{\partial v}{\partial y}=0 \tag{2.62}$$

$$\begin{aligned} u\frac{\partial u}{\partial x}+v\frac{\partial u}{\partial y}&=\left(\nu_{hnf}+\frac{1}{\rho_{hnf}\beta\varsigma}\right)\frac{\partial^2 u}{\partial y^2}-\frac{1}{2\beta\varsigma^3\rho_{hnf}}\left(\frac{\partial u}{\partial y}\right)^2\frac{\partial^2 u}{\partial y^2}\\ &-\frac{\sigma_{\mathrm{hnf}}B^2}{\rho_{\mathrm{hnf}}}u+\frac{\sigma B_0^2}{\rho C_p}u+g\beta_{hnf}\left(T-T_\infty\right)-\frac{\mu_{hnf}}{\rho_{hnf}K_1}u \end{aligned} \tag{2.63}$$

$$u\frac{\partial T}{\partial x}+v\frac{\partial T}{\partial y}=\frac{k_{\mathrm{hnf}}}{(\rho C_p)_{\mathrm{hnf}}}\left[\frac{\partial^2 T}{\partial y^2}\right]-\frac{1}{(\rho C_p)_{\mathrm{hnf}}}\left[\frac{\partial q_r}{\partial y}\right] \tag{2.64}$$

subject to boundary conditions,

$$u=U\left(x\right),\quad v=0,\ T=T_\infty \text{ at } y=0 \tag{2.65}$$

$$u\ \to 0,\quad T\to T_\infty \quad \text{as } y\to\infty \tag{2.66}$$

The porous medium is defined by porous layer resists the flow with a drag proportional to the fluid's viscosity and inversely to the medium's permeability, $-\frac{\mu_{hnf}}{\rho_{hnf}K_1}u$ (Rashad et al., 2023). A thicker nanofluid slows the fluid more, warms it up, and usually cuts the heat-transfer rate. K_1 is Darcy permeability to represent Darcy's law which is a constitutive equation that describes fluid flow through porous media for Reynold numbers up to about 1 (Escudier & Atkins, 2019).

To obtain the ordinary differential equation (ODEs) from the model, similarity variables need to be implemented, which are given as (Hahim et al., 2023),

$$u = \frac{\partial \psi}{\partial y}, \quad v = -\frac{\partial \psi}{\partial x},$$
$$\eta(x,y) = \sqrt{\frac{c}{\nu_f}}\, y, \;\; \psi(x,y) = \sqrt{\nu_f c}\, x f(\eta), \tag{2.67}$$
$$\theta(\eta) = \frac{T - T_\infty}{T_w - T_\infty}$$

This similarity equations are necessary to converts a messy, coupled, time-dependent 2-D Newtonian boundary layer system into a boundary-value problem in η .

3.2 Thermophysical Properties and Characteristics

The thermophysical properties are given in Table 1 (Takabi & Salehi, 2014; Zainal et al., 2021),

Table 1: Formula of thermophysical properties for hybrid nanofluid

Thermophysical Properties	Hybrid Nanofluid Formula
Density	$\rho_{hnf} = (1-\phi_{hnf})\rho_f + \phi_1\rho_{s1} + \phi_2\rho_{s2}$
Dynamic Viscosity	$\frac{\mu_{hnf}}{\mu_f} = \frac{1}{(1-\phi_{hnf})^{2.5}}$
Heat Capacity	$(\rho c_p)_{hnf} = (1-\phi_{hnf})(\rho c_p)_f + \phi_1(\rho c_p)_{s1} + \phi_2(\rho c_p)_{s2}$
Electrical Conductivity	$\frac{\sigma_{hnf}}{\sigma_f} = \frac{\left(\frac{\phi_1\sigma_{s1}+\phi_2\sigma_{s2}}{\phi_{hnf}} + 2\sigma_f + 2(\phi_1\sigma_{s1}+\phi_2\sigma_{s2}) - 2\phi_{hnf}\sigma_f\right)}{\left(\frac{\phi_1\sigma_{s1}+\phi_2\sigma_{s2}}{\phi_{hnf}} + 2\sigma_f - (\phi_1\sigma_{s1}+\phi_2\sigma_{s2}) + \phi_{hnf}\sigma_f\right)}$
Thermal Conductivity	$\frac{k_{hnf}}{k_f} = \frac{\left(\frac{\phi_1 k_{s1}+\phi_2 k_{s2}}{\phi_{hnf}} + 2k_f + 2(\phi_1 k_{s1}+\phi_2 k_{s2}) - 2\phi_{hnf}k_f\right)}{\left(\frac{\phi_1 k_{s1}+\phi_2 k_{s2}}{\phi_{hnf}} + 2k_f - (\phi_1 k_{s1}+\phi_2 k_{s2}) + \phi_{hnf}k_f\right)}$
Thermal Expansion	$\beta_{hnf} = \frac{1}{\rho_{hnf}}\left[\phi_1\rho_1\beta_1 + \phi_2\rho_2\beta_2 + (1-\phi)\rho_f\beta_f\right]$

Table 1 summarizes the empirical and theoretical formulations used to compute the effective thermophysical properties of a hybrid nanofluid composed of two distinct nanoparticles (Cu and Al_2O_3) dispersed in a base fluid such as ethylene glycol (EG).

These properties are derived from mixture theory and modified Maxwell-Garnett correlations.

The formulations incorporate volume fractions (ϕ_1, ϕ_2) and the intrinsic properties of the base fluid and solid nanoparticles, ensuring that the resulting hybrid nanofluid reflects the combined influence of both solid components. This table provides the fundamental property framework for substituting realistic hybrid fluid parameters into the Powell-Eyring governing equations, allowing accurate prediction of momentum and heat transfer behaviours in subsequent numerical simulations

The thermophysical characteristics are given in Table 2 (Aziz et al., 2021),

Table 2: Formula of thermophysical characteristics for hybrid nanofluid

Thermophysical Char.	ρ **(kg/m)**	c_p **(J/kg·K)**	k **(W/m·K)**	σ **(S/m)**
Ethylene glycol (EG)	1114	2415	0.252	5.5×10^{-6}
Copper (Cu)	8933	385.0	401.00	5.96×10^{7}
Alumina (Al_2O_3)	3970	765.0	40.000	3.5×10^{7}

Table 2 lists the measured thermophysical characteristics of the base fluid and the nanoparticles used in constructing the hybrid nanofluid model. It provides the essential material constants for ethylene glycol (EG), copper (Cu), and alumina (Al_2O_3), which are later substituted into the hybrid formulations presented in Table 1.

These values form the physical foundation for calculating the effective hybrid nanofluid properties through the corresponding mixture relations. For instance, the high thermal and electrical conductivities of Cu significantly boost the overall energy transport capability, while Al_2O_3 enhances the fluid's stability and viscosity. Meanwhile, EG serves as the base fluid providing good thermal capacity and low volatility. Together, the table quantifies how combining Cu-Al_2O_3 nanoparticles in EG yields an optimized balance of heat conduction, energy storage, and flow stability, thereby supporting the numerical modelling of Powell-Eyring hybrid nanofluid flows under magnetic and radiative effects.

3.3 Numerical computation

Shampine et al. (2000) present an extensive tutorial on solving two-point and multipoint boundary value problems (BVPs) using MATLAB's bvp4c solver. Unlike initial value problems (IVPs), BVPs specify boundary conditions at more than one point, and may admit multiple, single, or no solutions. The paper provide step by step implementation, explains that effective BVP solvers require initial guesses for both the solution and any unknown parameters, emphasizing the necessity of well-conditioned numerical formulations for convergence.

The reduced ODEs will be solved numerically using MATLAB's boundary value problem solver, as guided by Shampine et al. (2000). However, instead of employing bvp4c, this research adopts an improved approach using the bvp5c solver, which is based on the embedded formula of the four-stage Lobatto IIIA method from the Runge-Kutta family. The computational flow is given as shown in Figure 9,

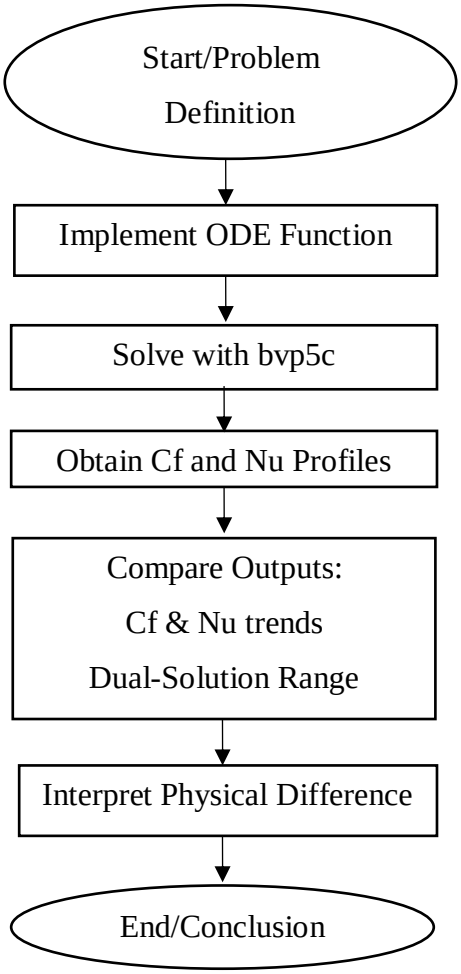

Figure 9: Methodological flow chart

Figure 9 illustrates the computational workflow adopted in this study for solving the reduced ordinary differential equations (ODEs) derived from the Powell-Eyring hybrid nanofluid models under various boundary conditions. The process begins with the problem definition and formulation of the ODE system representing the physical flow configuration. These equations are then implemented into MATLAB as an ODE function, along with the corresponding boundary conditions and initial guesses. The bvp5c solver, a fifth-order, adaptive, collocation-based method from the Runge-Kutta family, is used to numerically compute velocity and temperature profiles. From these solutions, the skin-friction coefficient (Cf) and Nusselt number (Nu) are extracted to evaluate the flow and thermal performance. The results are subsequently compared and interpreted to identify dual-solution regions and assess the physical behaviour of each parameter, culminating in the conclusion of the numerical study.

3.3.1 Boundary Value Problem Fifth-Order Method (BVP5C) by MATLAB

The MATLAB solver bvp5c requires three main inputs an ODE function, a boundary condition function, and an initial solution along with one optional input for solver settings. The ODE function (odefun) must be written as a system of first-order equations in matrix form, representing the reduced velocity, f and temperature θ, profiles up to their highest derivatives. The boundary condition function (bcfun) specifies the constraints at the domain boundaries, $g\left(y(a), y(b)\right) = 0$ while the initial solution (solinit) provides a starting guess for the solver, typically generated using the bvpinit function, which requires a mesh for the similarity variable (η) and a set of guessed solution values matching the structure of the ODE system. The optional fourth input is an options structure created with bvpset, which allows the user to adjust solver tolerances, mesh refinement, and maximum iterations. Once these components are defined, bvp5c iteratively refines the solution until both the governing equations and boundary conditions are satisfied within the specified tolerance. The resulting solution can then be post-processed and visualized to analyse velocity and temperature distributions, skin-friction coefficients, Nusselt numbers, or other quantities of interest.

3.3.2 Backward Differentiation Formula (BDF)

In implementation, the method begins with known initial values, constructs the block system for the next steps, and iteratively refines the solutions until convergence is achieved within a specified tolerance. BDF is used alongside MATLAB's bvp5c to provide a comparative framework: while bvp5c is a collocation-based boundary-value solver, we solve the boundary-value system via a shooting procedure that treats the unknown wall data as parameters and integrates the resulting IVP with a fourth-order, A-stable two-point BDF scheme; the shooting parameters are updated by Newton's method until the far-field conditions $f'(\eta_{max}) = u_{\infty}^{*}$ and $\theta(\eta_{max}) = 0$ are satisfied within tolerance.

The two-point BVP will be converted into an initial value problem via the shooting method. Provide initial guess the missing initial condition at the wall (such as the asymptotic far-field value of velocity or temperature gradient), integrate the ODEs

from the wall outward using a ODE solver (like an adaptive BDF integrator), and adjust the guess until the far-field boundary condition is satisfied. In the shooting approach, using a solver is crucial because the domain is typically $y \in [0, \infty)$ and the solution decays exponentially (an explicit integrator would require tiny steps to capture that decay) whereas an implicit BDF can march with larger steps and remain stable. BDF-based integrators also handle well the "dual-scale" nature of some solutions (for instance, if a thin boundary layer is present within a larger domain). Researchers have indeed combined BDF integrators with shooting: for example, Rezaee & Houshmand (2023) solved a non-similar unsteady boundary layer flow by first using a fourth-order Runge-Kutta for the initial portion and then switching to a BDF method near the separation point to continue integration. This hybrid approach ensured stability close to the singular point where RK4 would fail. The s-step BDF is given as:

$$y_{n+1} - y_n = hf\left(t_{n+1}, y_{n+1}\right) \tag{2.68}$$

which is also called backward Euler method.

The initial value problem to solve is (James Audu et al., 2022),

$$y^{(iv)} = f\left(x, y, y', y'', y'''\right) \tag{2.69}$$

where f is a continuous real-valued function involving its first, second, and third derivatives, subject to the following initial conditions:

$$y(x_0) = y_0,\ y'(x_0) = y_0',\ y''(x_0) = y_0'',\ \ y'''(x_0) = y_0''' \tag{2.70}$$

The general formula for BDF is given as:

$$f\left(x, y, y', y'', y'''\right) = \sum_{j=0}^{d+c-1} j(j-1)(j-2)(j-3) g_j x^{j-4} \tag{2.71}$$

where d and c are numbers of interpolation and collocation points respectively, $x \in [x_0, x_N]$, and g_j are unknown coefficients to be determined by resolving a system of 13×13 system of nonlinear algebraic equations in a form of $KX = B$ generated from,

$$\begin{aligned}
&Y\left(x_{m+j}\right) = y_{m+j} \\
&Y'\left(x_{m+j}\right) = y'_{m+j} \\
&Y''\left(x_{m+j}\right) = y''_{m+j} \\
&Y'''\left(x_{m+j}\right) = y'''_{m+j} \\
&j = 0, \frac{1}{8}, \frac{1}{4}, \frac{3}{8}, \frac{1}{2}, \frac{5}{8}, \frac{3}{4}, 1, \frac{9}{8}, \frac{5}{4}, \frac{3}{2}, \frac{7}{4}, 2
\end{aligned} \tag{2.72}$$

By using the inversion of matrix method, the value of g_j are obtained and inserted into to get the continuous scheme of the BDF as,

$$\begin{aligned}
y(x) = {} & \alpha_0 y_m + \alpha_{\frac{1}{8}}(x) y_{m+\frac{1}{8}} + \alpha_{\frac{1}{4}}(x) y_{m+\frac{1}{4}} + \alpha_{\frac{3}{8}}(x) y_{m+\frac{3}{8}} \\
& + \alpha_{\frac{1}{2}}(x) y_{m+\frac{1}{2}} + \alpha_{\frac{5}{8}}(x) y_{m+\frac{5}{8}} + \alpha_{\frac{3}{4}}(x) y_{m+\frac{3}{4}} \\
& + \alpha_1(x) y_{m+1} + \alpha_{\frac{9}{8}}(x) y_{m+\frac{9}{8}} + \alpha_{\frac{5}{4}}(x) y_{m+\frac{5}{4}} \\
& + \alpha_{\frac{3}{2}}(x) y_{m+\frac{3}{2}} + \alpha_{\frac{7}{4}}(x) y_{m+\frac{7}{4}} + h^4 \beta_2(x) f_{m+2}
\end{aligned} \tag{2.73}$$

Evaluating (2.73) then gives the required schemes to implement block mode and get the numerical result.

CHAPTER 4
RESEARCH ACTIVITY

4.1 Project Gantt Chart

Table 3 outlines the overall timeline of research activities across the duration of the project:

Table 3: Project Gantt Chart

Year	2025										2026							
Months	3	4	5	6	7	8	9	10	11	12	1	2	3	4	5	6	7	8
Mathematical Modelling																		
Numerical Solution																		
Data Analysis																		
Writing Report																		

4.2 Project Milestone and Dates

Table 4 provides the key milestones and corresponding deadlines for each major research stage:

Table 4: Project Milestone and Dates

RESEARCH ACTIVITIES	START DATE	END DATE
LITERATURE REVIEW	24/3/2025	19/9/2026
RESEARCH PROPOSAL	24/3/2025	23/9/2025
RESEARCH ETHICS	23/9/2025	22/11/2025
METHODOLOGY 1	22/6/2025	21/10/2025
METHODOLOGY 2	21/10/2025	19/2/2026

METHODOLOGY 3	19/2/2026	21/6/2026
THESIS WRITING	23/9/2025	19/9/2026
THESIS EXAMINATION	19/9/2026	28/11/2026
THESIS CORRECTION	28/11/2026	26/2/2027
REGISTERED	24/3/2025	
DEFENSE RESEARCH PROPOSAL	23/9/2025	
RESEARCH ETHICS APPROVED	22/11/2025	
RESEARCH OBJECTIVE 1	21/10/2025	
RESEARCH OBJECTIVE 2	19/2/2026	
RESEARCH OBJECTIVE 3	21/6/2026	
THESIS SUBMITTED	19/9/2026	
VIVA VOCE	28/11/2026	
STUDY COMPLETED	23/3/2027	

REFERENCES

Abolbashari, M. H., Freidoonimehr, N., Nazari, F., & Rashidi, M. M. (2014). Entropy analysis for an unsteady MHD flow past a stretching permeable surface in nano-fluid. *Powder Technology, 267*, 256–267. https://doi.org/10.1016/j.powtec.2014.07.028

Adun, H., Wole-Osho, I., Okonkwo, E. C., Kavaz, D., & Dagbasi, M. (2021). A critical review of specific heat capacity of hybrid nanofluids for thermal energy applications. *Journal of Molecular Liquids, 340*. https://doi.org/10.1016/j.molliq.2021.116890

Aljabali, A., Kasim, A. R. M., Waini, I., Khashi'ie, N. S., & Tijani, Y. O. (2025). Thermal Analysis of Eyring-Powell Hybrid Nanofluid: A Case of Combined Convective Transport and Radiative Heat Flux along Inclined Stretching/Shrinking Sheet. *WSEAS Transactions on Heat and Mass Transfer, 20*, 1–13. https://doi.org/10.37394/232012.2025.20.1

Alrashdi, A. M. A. (2023). Mixed convection and thermal radiation effects on non-Newtonian nanofluid flow with peristalsis and Ohmic heating. *Frontiers in Materials, 10*. https://doi.org/10.3389/fmats.2023.1178518

Aminuddin, N. A. (2024). *Effects of non-newtonian hybrid nanofluid heat transfer and entropy generation over a horizontal shrinking surface* [Master Thesis]. Universiti Pertahanan Nasional Malaysia.

Aminuddin, N. A., Nasir, N. A. A. M., Jamshed, W., Abdullah, N., Ishak, A., Pop, I., & Eid, M. R. (2024). Velocity and thermal slip impact towards GO-MoS2/C3H8O3 hybridity nanofluid flowing via a moving Riga plate. *Ain Shams Engineering Journal, 15*(4). https://doi.org/10.1016/j.asej.2024.102648

Anuar, N. S., Bachok, N., & Pop, I. (2021). Influence of buoyancy force on Ag-MgO/water hybrid nanofluid flow in an inclined permeable stretching/shrinking sheet. *International Communications in Heat and Mass Transfer, 123*. https://doi.org/10.1016/j.icheatmasstransfer.2021.105236

Asshaari, I., & Md Jedi, M. A. (2022). *Nanobendalir Mono dan Hibrid Pendekatan Statistik dalam Mekanik Bendalir* (1st ed.). Penerbit Universiti Kebangsaan Malaysia.

Aziz, A., Jamshed, W., Aziz, T., Bahaidarah, H. M. S., & Ur Rehman, K. (2021). Entropy analysis of Powell–Eyring hybrid nanofluid including effect of linear

thermal radiation and viscous dissipation. *Journal of Thermal Analysis and Calorimetry*, *143*(2), 1331–1343. https://doi.org/10.1007/s10973-020-10210-2

Badruddin, I. A., & Quadir, G. A. (2016). Heat transfer in porous medium embedded with vertical plate: Non-equilibrium approach - Part A. *AIP Conference Proceedings*, *1738*. https://doi.org/10.1063/1.4952360

Bibi, S. K. N., Padma, G., & Sailaja, P. (2023). Soret effect on an unsteady MHD free convective flow past an infinite vertical plate with constant suction. *Materials Today: Proceedings*, *92*, 1518–1525. https://doi.org/10.1016/j.matpr.2023.05.723

Challa, K. K., Rao, M. E., Jawad, M., Saidani, T., Ali Osman Abdallah, S., & D, T. (2025). Enhanced heat transfer and flow dynamics of Powell-Eyring nanofluid: unsteady stretched surface and with Stefan blowing/suction. *Case Studies in Thermal Engineering*, *65*. https://doi.org/10.1016/j.csite.2024.105664

Earl, R., & Nicholson, J. (2021). *The Concise Oxford Dictionary of Mathematics* (6th ed.). Oxford University Press. https://doi.org/10.1093/acref/9780198845355.001.0001

Escudier, M., & Atkins, T. (2019). *A Dictionary of Mechanical Engineering*. Oxford University Press. https://doi.org/10.1093/acref/9780198832102.001.0001

Hahim, Bouzgarrou, S., Rehman, S., & Sabi, E. (2023). Thermodynamic analysis of Powell-Eyring-blood hybrid nanofluid through vertical stretching sheet with interface slip and melting heat. *Results in Engineering*, *20*. https://doi.org/10.1016/j.rineng.2023.101644

Hayat, T., Ali, S., Alsaedi, A., & Alsulami, H. H. (2016). Influence of thermal radiation and Joule heating in the Eyring–Powell fluid flow with the Soret and Dufour effects. *Journal of Applied Mechanics and Technical Physics*, *57*(6), 1051–1060. https://doi.org/10.1134/S0021894416060122

Hayat, T., Asad, S., Mustafa, M., & Alsaedi, A. (2014). Radiation effects on the flow of powell-eyring fluid past an unsteady inclined stretching sheet with non-uniform heat source/sink. *PLoS ONE*, *9*(7). https://doi.org/10.1371/journal.pone.0103214

James Audu, K., Garba, J., Tunde Tiamiyu, A., & Ashiodime Thomas, B. (2022). Application of Backward Differentiation Formula on Fourth-Order Differential Equations. *JOURNAL OF SCIENCE AND TECHNOLOGY*, *14*(2), 52–65. https://doi.org/10.30880/jst.2022.14.02.006

Jamshed, W., Eid, M. R., Nisar, K. S., Nasir, N. A. A. M., Edacherian, A., Saleel, C.

A., & Vijayakumar, V. (2021). A numerical frame work of magnetically driven Powell-Eyring nanofluid using single phase model. *Scientific Reports*, *11*(1). https://doi.org/10.1038/s41598-021-96040-0

Jusoh, R., Ismail, Z., Mohamed, M. K. A., & Zainuddin, N. (2024). Magnetohydrodynamics Cu-TiO2 Hybrid Nanofluid with Viscous Dissipation. In S. Shafie & L. Y. Jiann (Eds.), *Hybrid Nanofluids and Its Model Applications* (1st ed., pp. 35–62). Penerbit UTM Press.

Khan, M. S., Abid, M., Yan, M., Ratlamwala, T. A. H., & Mubeen, I. (2021). Thermal and thermodynamic comparison of smooth and convergent-divergent parabolic trough absorber tubes with the application of mono and hybrid nanofluids. *International Journal of Energy Research*, *45*(3), 4543–4564. https://doi.org/10.1002/er.6123

Khan, N. A., Sultan, F., & Khan, N. A. (2015). Heat and mass transfer of thermophoretic MHD flow of powell-eyring fluid over a vertical stretching sheet in the presence of chemical reaction and joule heating. *International Journal of Chemical Reactor Engineering*, *13*(1), 37–49. https://doi.org/10.1515/ijcre-2014-0090

Krishna, P. M., Sandeep, N., Reddy, J. V. R., & Sugunamma, V. (2016). Dual solutions for unsteady flow of Powell-Eyring fluid past an inclined stretching sheet. *Journal of Naval Architecture and Marine Engineering*, *13*(1), 89–99. https://doi.org/10.3329/jname.v13i1.25338

Law, J., & Rennie, R. (2020). *A Dictionary of Chemistry*. Oxford University Press. https://doi.org/10.1093/acref/9780198841227.001.0001

Madhesh, D., & Kalaiselvam, S. (2014). Experimental analysis of hybrid nanofluid as a coolant. *Procedia Engineering*, *97*, 1667–1675. https://doi.org/10.1016/j.proeng.2014.12.317

Maiti, H., & Mukhopadhyay, S. (2025). Insight into Eyring–Powell nanofluid flow over a radially stretching disk with Stefan blowing, nonlinear thermal radiation and Newtonian heating. *Multiscale and Multidisciplinary Modeling, Experiments and Design*, *8*(6). https://doi.org/10.1007/s41939-025-00860-w

Majumdar, P. (2021). *Computational Fluid Dynamics and Heat Transfer* (2nd ed.). CRC Press. https://books.google.com.my/books?id=uF5QEAAAQBAJ

Mane, N. S., & Hemadri, V. (2022). Experimental Investigation of Stability, Properties and Thermo-rheological Behaviour of Water-Based Hybrid CuO and

Fe3O4 Nanofluids. *International Journal of Thermophysics*, *43*(1). https://doi.org/10.1007/s10765-021-02938-2

Manimaran, M., Norizan, M. N., Kassim, M. H. M., Adam, M. R., Abdullah, N., & Norrrahim, M. N. F. (2025). Critical review on the stability and thermal conductivity of water-based hybrid nanofluids for heat transfer applications. In *RSC Advances* (Vol. 15, Issue 18, pp. 14088–14125). Royal Society of Chemistry. https://doi.org/10.1039/d5ra00844a

Mohamad, N., Khan, U., & Ishak, A. (2024). Assessing the Efficacy of Hybrid Nanofluid within a Non-Newtonian Reiner-Philippoff Model, Incorporating MHD and Thermal Radiation Past a Stretching/Shrinking Sheet. *PaperASIA*, *40*(4b), 165–177. https://doi.org/10.59953/paperasia.v40i4b.199

Muhammad, T., Waqas, H., Khan, S. A., Ellahi, R., & Sait, S. M. (2021). Significance of nonlinear thermal radiation in 3D Eyring–Powell nanofluid flow with Arrhenius activation energy. *Journal of Thermal Analysis and Calorimetry*, *143*(2), 929–944. https://doi.org/10.1007/s10973-020-09459-4

Nabwey, H. A., Armaghani, T., Azizimehr, B., Rashad, A. M., & Chamkha, A. J. (2023). A Comprehensive Review of Nanofluid Heat Transfer in Porous Media. In *Nanomaterials* (Vol. 13, Issue 5). MDPI. https://doi.org/10.3390/nano13050937

Naseem, T., Bibi, I., Shahzad, A., & Munir, M. (2023). Analysis of Heat Transport in a Powell-Eyring Fluid with Radiation and Joule Heating Effects via a Similarity Transformation. *Fluid Dynamics and Materials Processing*, *19*(3), 663–677. https://doi.org/10.32604/fdmp.2022.021136

Norzawary, N. H. A., Soid, S. K., Ishak, A., Anuar Mohamed, M. K., Khan, U., Sherif, E. S. M., & Pop, I. (2023). Stability analysis for heat transfer flow in micropolar hybrid nanofluids. *Nanoscale Advances*, *5*(20), 5627–5640. https://doi.org/10.1039/d3na00675a

Parmar, A., Kumar, P., Choudhary, R., Garg, S., & Jain, A. (2024). Unsteady Inclined MHD Powell-Eyring Fluid with Microorganisms Over an Inclined Permeable Stretching Sheet with Zero Mass Flux and Slip Condition. *International Journal of Applied and Computational Mathematics*, *10*(5). https://doi.org/10.1007/s40819-024-01780-y

Rashad, A. M., Nafe, M. A., & Eisa, D. A. (2023). Heat Generation and Thermal Radiation Impacts on Flow of Magnetic Eyring–Powell Hybrid Nanofluid in a

Porous Medium. *Arabian Journal for Science and Engineering*, *48*(1), 939–952. https://doi.org/10.1007/s13369-022-07210-9

Rennie, R., & Law, J. (2019). *A Dictionary of Physics*. Oxford University Press. https://doi.org/10.1093/acref/9780198821472.001.0001

Rezaee, V., & Houshmand, A. (2023). NUMERICAL SOLUTION OF NON-SIMILAR BOUNDARY-LAYER FLOW OVER A CYLINDER. *Journal of the Serbian Society for Computational Mechanics*, *17*(1), 134–150. https://doi.org/10.24874/jsscm.2023.17.01.10

Rohsenow, W. M. ., Hartnett, J. P. ., & Cho, Y. I. . (1998). *Handbook of heat transfer*. McGraw-Hill.

Saleh, B., & Sundar, L. S. (2021). Thermal efficiency, heat transfer, and friction factor analyses of mwcnt + fe3o4/water hybrid nanofluids in a solar flat plate collector under thermosyphon condition. *Processes*, *9*(1), 1–19. https://doi.org/10.3390/pr9010180

Shampine, L. F., Kierzenka, J., & Reichelt, M. W. (2000). *Solving Boundary Value Problems for Ordinary Differential Equations in Matlab with bvp4c*.

Suresh, S., Venkitaraj, K. P., Selvakumar, P., & Chandrasekar, M. (2012). Effect of Al 2O 3-Cu/water hybrid nanofluid in heat transfer. *Experimental Thermal and Fluid Science*, *38*, 54–60. https://doi.org/10.1016/j.expthermflusci.2011.11.007

Tabassum, R., & Mehmood, R. (2020). Crosswise Transport Mechanism of Micro-rotating Hybrid (Cu–Al2O3/H2O) Nanofluids Through Infusion of Various Shapes of Nanoparticles. *Arabian Journal for Science and Engineering*, *45*(7), 5883–5893. https://doi.org/10.1007/s13369-020-04580-w

Takabi, B., & Salehi, S. (2014). Augmentation of the heat transfer performance of a sinusoidal corrugated enclosure by employing hybrid nanofluid. *Advances in Mechanical Engineering*, *2014*. https://doi.org/10.1155/2014/147059

Wahid, N. S., Arifin, N. M., Khashi'ie, N. S., & Pop, I. (2023). Mixed convection MHD hybrid nanofluid over a shrinking permeable inclined plate with thermal radiation effect. *Alexandria Engineering Journal*, *66*, 769–783. https://doi.org/10.1016/j.aej.2022.10.075

Zainal, N. A., Nazar, R., Naganthran, K., & Pop, I. (2021). Unsteady MHD stagnation point flow induced by exponentially permeable stretching/shrinking sheet of hybrid nanofluid. *Engineering Science and Technology, an International Journal*, *24*(5), 1201–1210. https://doi.org/10.1016/j.jestch.2021.01.018

Zainal, N. A., Nazar, R., Pop, I., & Naganthran, K. (2024). Unsteady Separated Hybrid Stagnation Nanofluid Flow. In S. Shafie & L. Y. Jiann (Eds.), *Hybrid Nanofluids and Its Model Applications* (1st ed., pp. 63–78). Penerbit UTM Press.

Zaman, H., Shah, M. A., & Ibrahim, M. (2013). Unsteady Incompressible Couette Flow Problem for the Eyring-Powell Model with Porous Walls. *American Journal of Computational Mathematics*, *03*(04), 313–325. https://doi.org/10.4236/ajcm.2013.34041

AUTHOR'S PROFILE

Nur Arif Husaini Bin Norwaza obtained Bachelor of Science (Hons.) Computational Mathematics in June 2021 from Universiti Teknologi MARA. Arif's broader interests span numerical analysis, scientific computing, AI-driven optimisation, and the design of enterprise-scale web architectures. He has published in peer-reviewed journals on applied mathematics and contributes to industrial projects that integrate Laravel, Nuxt.js and PostgreSQL back ends. Passionate about knowledge transfer, he frequently mentors' junior developers and leads workshops on advanced coding patterns and data-driven problem solving.